Data Center Power System Stability – Part II: System Modeling and Analysis

Jian Sun, *Fellow, IEEE*, Melaku Mihret, Mauricio Cespedes, David Wong, and Mike Kauffman

***Abstract*—This is the second part of a two-part paper on stability study of data center power systems by impedance-based methods. As the basis for this application, Part I [1] developed new impedance models for power supplies that are the most dominant loads in data centers. This second part presents system modeling and analysis methods that can support practical data center power system design to ensure stability. The proposed methods comprise: 1) building distribution network modeling by impedance scaling; 2) system modeling and model reduction based on equivalent source impedance; 3) system stability analysis in the sequence domain to include zero-sequence dynamics; and 4) expansion of system models and analyses to account for network asymmetry and uneven loading. These methods are used to characterize practical resonance problems observed in data centers, explain their root causes, and develop solutions. For systems using Y-connected power supply units (PSUs), the zero sequence is identified as the weakest link and the first to become unstable. The expanded system model and analysis reveal a new, differential-mode instability that is responsible for high frequency resonances. To guarantee system stability, new impedance-based product and system design specifications are developed based on sufficient conditions derived from the Nyquist stability criterion. Laboratory and field measurements are presented to substantiate the proposed methods and conclusions.**

***Index Terms*—Data center power systems, frequency-domain methods, impedance modeling, system stability, system resonance.**

I. Introduction

DATA centers have evolved from serving dedicated customers and functions to being the hub of the growing IT infrastructure that people in many parts of the world depend on for everyday life [2]. Maintaining continuous operation of a data center is critical and requires uninterrupted power supply. On the other hand, building a highly reliable power system for a modern data center that consumes hundreds of megawatts of power is a capital-intensive investment. Since electricity consumption constitutes the largest percentage of data center's operational cost, system energy efficiency is also critical.

A major driver for cost and inefficiency of traditional IT power system is the use of AC uninterruptible power supplies (UPS). DC power distribution has been proposed as an alternative [3] and promises to reduce overall cost [4]. However, AC distribution remains the industry standard to date. New AC distribution architectures have also been developed to improve efficiency and reduce cost. One example is the Open Compute Project (OCP) architecture that largely eliminates the use of AC UPS by powering most server racks directly from the utility grid through a 480 V distribution network [5]. Meta data centers are built based on this architecture.

Stability considerations for IT power systems have traditionally focused on minimizing the output impedance of UPS [6], [7]. In the new OCP architecture mentioned above, minimizing the UPS output impedance is still important, but only helps the stability of a small number of power supplies. Most server power supplies are powered directly from the utility grid without UPS, such that their stability is affected by the grid impedance. While most data centers are built to have a strong grid connection, the sheer number and total power consumption of power supplies in a large data center in effect creates a "weak-grid" environment that is known to cause instability for grid-connected converters in other industry. The operation of most servers from a single (utility) source also means that an instability event would affect all of them at the same time, potentially causing much severer consequences than the failure of any number of power supply units (PSUs) or a UPS would do. Ensuring stability is therefore a critical requirement for the design and operation of modern data center power systems.

This two-part work was motivated by actual resonance events in Meta data centers. The Introduction of Part I [1] described two types of resonances between server PSUs and the distribution network. They are considered new because their behavior and root causes are different from typical instability phenomena involving power supplies. On the other hand, they closely resemble the stability problems in renewable energy and high-voltage DC (HVDC) systems. A common root cause, for example, is the negative damping in a converter's impedance near the fundamental frequency due to internal DC bus voltage control and other effects, as well as at high frequency due to control delays. Negative damping near the fundamental frequency can cause low-frequency resonance when the grid impedance is high. This is a common problem for large-scale wind and PV systems [8], [10], and is identified as the root cause for the low frequency resonance described in Part I. On the other hand, delay-induced negative damping is responsible for high-frequency resonances [11], [13]. (Refer to Section II of Part I for the definition of low-, medium- and

Manuscript received March 20, 2021; revised May 28, 2021; accepted November 12, 2021. Date of online publication February 14, 2022; date of current version February 23, 2022.

J. Sun (corresponding author, e-mail: jsun@rpi.edu; ORCID: https://orcid.org/0000-0001-8820-5593) is with Rensselaer Polytechnic Institute – ECSE, 110 8th Street Room CII 8015 , Troy 12180, United States.

M. Mihret, M. Cespedes, D. Wong and M. Kauffman are with Meta Platforms Inc., 1601 Willow Rd, Menlo Park, California 94025-1452, United States.

DOI: 10.17775/CSEEJPES.2021.02020

high-frequency ranges used in this work.)

Impedance modeling and analysis is an effective method to study converter-grid system stability [14]. Server power supplies are the most dominant and important loads in data centers. To support impedance-based modeling and analysis of data center power system stability, Part I of the work presented new impedance models for single-phase power supply units (PSUs) and its operation with a single-phase source to explain how negative damping in the PSU impedance leads to low and high frequency resonances. The analyses provided general directions to improve PSU design that can enhance system stability. The focus of Part II is impedance modeling and analysis of overall data center power systems for the same purpose. The goal is to relate the architecture and different parameters of the power system to stability requirements such that they can be designed to ensure system stability.

The impedance-based stability criterion presented in [14] treated the grid as an ideal voltage source behind an impedance. This model has been used in almost all subsequent works on the subject. For a wind or PV farm [10], an HVDC converter [12], or an electric locomotive [15], definition of the grid impedance is rather straightforward, and an impedance model can be built based on the short-circuit ratio (SCR) and X/R ratio of the transmission/distribution lines. Such an RL model is usually sufficient for the study of converter-grid stability below the first (parallel) resonance frequency in the grid impedance. When multiple converters are involved, such as in a wind or PV farm, impedances of individual converters and the network connecting them can be aggregated to define an equivalent impedance representing all converters and used against the impedance of the grid measured at the point of common coupling (PCC) to determine system stability. The aggregation can also include the coupled current responses [16]. Alternatively, the grid impedance measured at the PCC can be scaled up by the number of converters operating in parallel to define an equivalent grid impedance for each converter and used against the converter impedance to assess stability. Recently, there were also efforts to extend the grid impedance concept to converters connected to multiple voltage sources through a meshed transmission network [17].

However, none of these methods can be directly applied to data centers. Aggregation assumes there is no instability among the converters that are aggregated. As alluded to early in this section, the "weak grid" environment in a data center is mostly due to the impedance of the power distribution system within the data center instead of the external grid, and instability is still a concern even if the grid is an ideal voltage source. Aggregation will miss the internal instability problem.

Power distribution in data centers employs a tree-like radial network, as shown in Fig. 1 presented in Section II. The source impedance seen by an individual PSU includes the impedance of different parts of the distribution network that are shared by PSUs in parallel branches. Scaling can be applied to find an equivalent source impedance for each PSU but requires a more general formulation in order to handle the complex multilayer architecture. An additional complexity is that the distribution network is in three phase while each PSU operates with a single-phase input, using either phase-neutral or phase-phase voltage. Because of phase coupling, the impedance of each segment of the distribution network is shared by not only PSUs of the same phase in parallel branches, but also PSUs of other phases of the same branch as well as other branches.

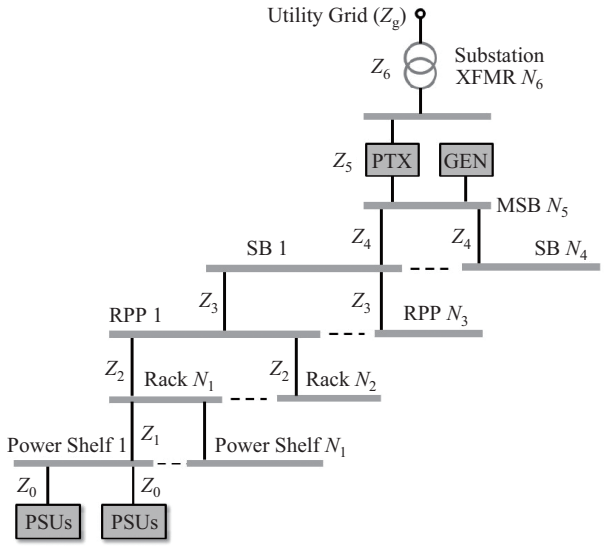

Fig. 1. Single-line diagram showing the architecture and key components of a data center power distribution system.

Our first objective for Part II of this paper is a systematic method to model data center power distribution network for system stability study based on impedance. The approach is to find an *equivalent source impedance* (ESI) that accounts for the complexities discussed above and can be used together with the PSU impedance models developed in Part I to form system stability models in single-input-single-output (SISO) form. A systematic method is developed to accomplish this in two steps:

- Reduce the multilayer radial distribution network to an equivalent three-phase source (with impedance) for a group of three PSUs in a Y or Δ configuration.
- Decompose the reduced three-phase source-PSU model into separate single-phase SISO models each involving the impedance of a single PSU and an equivalent source.

The second objective and contribution of this work is the understanding of how data center power system stability relates to the design of the building distribution network in general, including its architecture, protection schemes, component characteristics, physical construction, and operation procedure. This parallels the work presented in Part I for PSUs and is made possible by the SISO system model and stability analysis. One conclusion we draw from the analysis is that zero sequence is the weakest link in Y-configured systems. Accordingly, methods to reduce zero-sequence impedance of the distribution network are proposed. A new differential-mode instability mode involving only a portion of the distribution network is also identified and used to explain the root causes for the high-frequency resonance reported in Part I.

The third objective and contribution of this work is the development of impedance-based performance specifications that can ensure system stability. Design for system stability

based on impedance has been researched in power electronics since the 1980s [18] but with very limited practical application. The Swiss Federal Railways (SBB) adopted this approach in early 2000s to prevent instability in railway electrical systems [19]. Based on the models and methods presented in Part I and II, we have developed such specifications for Meta data centers [20], [22]. The requirements are comprehensive and can be a useful reference for other industries. In collaboration with Meta suppliers, the team also demonstrated technologies and design methods to comply with the new requirements. The methodology we applied to develop the specifications and the rationale behind the requirements are reviewed in this paper.

The remaining of the paper is organized as follows: Section II reviews the architecture of data center power systems and the PSU models developed in Part I. A generalized scaling method is then introduced and used to define an equivalent source impedance model for a group of three PSUs. This model is used in Section III in conjunction with the PSU impedance models presented in Part I to develop a three-phase system impedance model that can be used to study system stability. The three-phase model is an extension of the SISO model presented in Part I and includes the coupled current responses of each PSU. To avoid the need for the generalized Nyquist criterion, Section IV applies symmetrical component analysis to convert the three-phase model into independent single-phase models, each in an SISO form. The models are used to characterize system stability at low frequency and show that zero sequence is the bottleneck in systems that use Y-connected PSUs. Methods to improve zero sequence stability are then discussed. Section V presents an expanded system model to account for factors ignored in the ESI model and uses it to explain the effects of network asymmetry and uneven loading on system stability as well as to identify a new differential-mode instability that is responsible for system resonance in the high-frequency range. Section VI presents laboratory and field measurements to substantiate the presented methods and findings. Development of impedance-based specifications for Meta data centers is also reviewed. Section VII summarizes the work.

II. System Architecture and Impedance Modeling

A. Data Center Power System Architecture

Meta data centers are designed using an integrated approach to achieve high energy efficiency and reliability. The power distribution network in a typical Meta data center employs the radial system depicted in Fig. 1. The design is made public through OCP [3]. The system starts from a utility transmission line feeding the data center at high voltage (e.g. 110 kV or 220 kV). The transmission voltage is stepped down to a medium voltage (e.g. 13.2 kV) by one of several substation transformers. This voltage is then stepped down further to a low voltage (e.g. 480 V) by a number of pad-mounted transformers (PTX) each powering a main switchboard (MSB). Each MSB is also supplied from a backup diesel generator (GEN), and can receive power from another, so-called reserve MSB (MSB-R), which is part of the $N+1$ block redundant electrical system design [3] and is not shown in Fig. 1.

From each MSB, the power branches out to a number of smaller switchboards (SB). Each SB in turn feeds a number of reactive power panels (RPPs), and each RPP feeds a row of server racks. The RPP includes series inductors to limit the fault current and to provide additional filtering to harmonics. Each server rack supplies power to a number of power supply units (PSUs) arranged in one or more power shelves. These PSUs convert the AC input to 12 or 48 V DC using a power-factor corrected (PFC) front end and an isolated DC-DC converter. The single-line diagram in Fig. 1 shows this radial architecture and its key components. The diagram also defines two sets of parameters that will be used in the system model:

- The impedance of each segment of the distribution system, indicated next to the line representing the segment (e.g. Z_2 is the impedance from a rack to a RPP, and Z_3 is the impedance from a RPP to an SB)
- The number of parallel branches at each level of the distribution system, indicated by the serial number of the last branch on the right (e.g. N_5 is the total number of MSBs connected to each substation transformer).

The PSUs in each power shelf form a three-phase group and are connected in either a delta (Δ) or star (Y) configuration, as depicted in Fig. 2. In the star configuration, a neutral line is also provided and each PSU operates between a phase and the neutral. This neutral is usually created at the secondary of the PTX. The line-line voltage is typically 480 V in the Y configuration and 208 V in the Δ configuration. The Δ configuration does not have the zero-sequence stability problem that is critical in the Y configuration, but tends to be less efficient because of the lower distribution voltage.

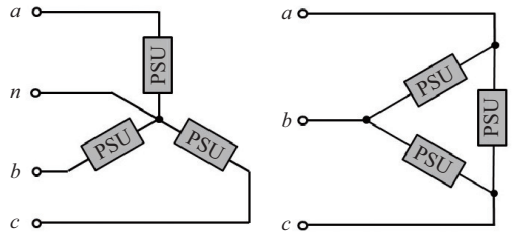

Fig. 2. Two different configurations of PSUs inside a server rack; left: star (Y) with neutral; right: delta (Δ).

B. PSU Impedance Models

Stability analysis of a converter-source system based on impedance requires an impedance model of the converter. For a PSU, the input impedance is the impedance of the PFC front-end converter with the DC-DC converter as its load. Part I [1] of the work presented new PFC converter input impedance models that can be used to study system stability in different frequency ranges. At low frequency, DC bus dynamics and the coupled current responses must be considered. The models developed in [1] for this application consist of three transfer functions (TF) describing the response of the PFC converter input current at three different frequencies when a small-signal voltage perturbation $\hat{v}_\mathrm{a}(s)$ is applied to the converter AC input:

1) A TF describing the current response $\hat{i}_\mathrm{a}$ at the perturba-

tion frequency s:

$$Y_{\rm a}(s) = \frac{\hat{i}_{\rm a}(s)}{\hat{v}_{\rm a}(s)} \tag{1}$$

2) A TF describing the current response at two times the fundamental ($\omega_1 = 2\pi f_1$) below the perturbation:

$$Y_{c-2}(s) = \frac{\hat{i}_{\rm a}(s - j2\omega_1)}{\hat{v}_{\rm a}(s)} \tag{2}$$

3) A TF describing the current response at two times the fundamental above the perturbation:

$$Y_{c+2}(s) = \frac{\hat{i}_{\rm a}(s + j2\omega_1)}{\hat{v}_{\rm a}(s)} \tag{3}$$

The coupled current response modeled by (2) and (3) are most significant below the second harmonic frequency ($2f_1$), especially near the fundamental. Above the second harmonic frequency, they can be ignored and (1) can be simplified to a medium-frequency model that includes only current control. Part I also presented a high-frequency model, which is essentially the medium-frequency model amended by

- A transfer function $e^{-sT_{\rm d}}$ added to the current compensator, $T_{\rm d}$ being the total control and PMW delay; and
- Impedance of the input EMI filter.

Since the low-frequency models (1)–(3) are most complex, we will focus on their use in the development of system model in the next section. Quantitative analyses in [1] have shown that the effects on the current at $s + j2\omega_1$ on converter-source stability are insignificant and can be ignored in practice. Based on that, the development in this part will consider the coupled current described by $Y_{c-2}(s)$ only. The developed models will be used for stability analysis in the medium- and high-frequency range by setting both coupling transfer functions to zero, and including control delay and filter impedance in $Y_{\rm a}(s)$.

C. Equivalent Three-Phase Source and Impedance

To form an SISO system impedance model, we need to find the equivalent source impedance seen by each PSU. With such an ESI, the PSU-source impedance model developed in Section IV of Part I can be used to represent the stability of the data center power system. As explained in the Introduction, this will be achieved in two steps. The first step is to find the ESI for a group of three PSUs in a three-phase configuration, which is presented in this subsection. As the starting point, we assume:

- The radial distribution network is symmetrical and each branch supplies the same number and type of PSUs as other parallel branches at the same layer.
- Other loads, such as UPS and mechanical loads, do not significantly affect stability and can be ignored.

Based on Meta data center design, these are deemed acceptable simplifications. The assumptions allow us to focus on the most dominant factors of system stability and capture them in a simple system model. A method to include network asymmetry, uneven loading, and other types of loads will be presented in Section V using an expanded system model.

The equivalent three-phase source impedance we look for will be determined by applying impedance scaling successively to each layer of the distribution network. The principle of this method can be explained as follows: Assume N identical PSUs are connected to a voltage source $v_{\rm s}$ behind impedance $Z_1(s)$, as depicted in Fig. 3(a), where $Z_0(s)$ is the impedance of the line from each PSU to the point of common coupling. Denote the input impedance of each PSU as $Z_l(s)$. Since the PSUs are identical, the N parallel branches can be lumped together and represented by one impedance that is equal to $N^{-1}Z_0(s) + N^{-1}Z_l(s)$. According to this equivalent circuit and the impedance-based stability criterion, the multi-PSU system is stable if each PSU is stable when operating with an ideal source and the following transfer function satisfies the Nyquist stability criterion:

$$l(s) = \frac{N^{-1}Z_0(s) + Z_1(s)}{N^{-1}Z_l(s)} \tag{4}$$

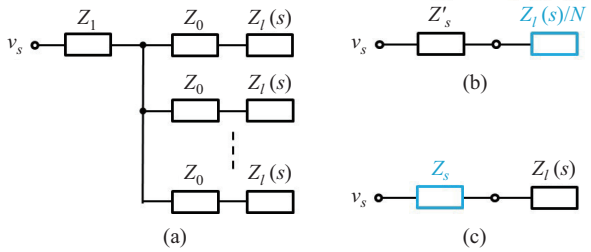

Fig. 3. (a) A multi-converter system, (b) simplification by aggregating the converters, and c) simplification by scaling source impedance.

The transfer function $l(s)$ defined in (4) can also be written as follows and be interpreted as the loop gain of an equivalent PSU-source system comprising one PSU connected to a source with N times the source impedance used in (4):

$$l(s) = \frac{Z_0(s) + NZ_1(s)}{Z_l(s)} \tag{5}$$

Eqs. (4) and (5) each in effect represents a general method to reduce a multi-converter system into a two-impedance system model for stability analysis: (4) is obtained by aggregating the converter impedances, and (5) by scaling the source impedance. Fig. 3(b) and (c) gives the corresponding equivalent circuits where $Z_{\rm s}(s) = NZ_1(s) + Z_0(s)$ and $Z'_{\rm s}(s) = Z_1(s) + Z_0(s)/N$. The scaling method defines the equivalent source impedance $Z_{\rm s}(s)$ seen by each converter in the system and is what we will use in this work.

The equivalent source impedance $Z_{\rm s}(s)$ used in Fig. 3(c) is essentially obtained by

- Multiplying the impedance of each segment of the network by the number of PSUs that connect through it to the source;
- Adding the scaled-up impedance of all segments in the path from a PSU to the source.

In this form, the method can be generalized to model the multilayer network depicted in Fig. 1. Using the symbols defined in the figure, we find the equivalent source impedance

for the PSU at the bottom of the diagram to be

$$Z_{\rm s}(s) = Z_0(s) + \sum_{i=1}^{6} \left\{ Z_i(s) \prod_{j=1}^{i} N_j \right\} \tag{6}$$

where N_j is the number of sub-lines that are powered from the line designated by impedance Z_j, $j = 1, 2, \ldots, 6$. For example, N_1 is the number of power shelves installed in each server rack, N_2 is the number of server racks powered from each RPP, N_3 is the number of RPPs powered from each SB, and N_6 is the number of substation transformers used in a data center.

As indicated early, the distribution network is actually a three-phase system. To model such a three-phase network, we first model each of its segments by a 3×3 or 4×4 impedance matrix depending on if the neutral is distributed. Each impedance matrix includes the self as well as the mutual impedance of the three phases (and the neutral). To apply the scaling method described by (6), we simply use the impedance matrix in place of the corresponding scalar impedance. The result is a 3×3 or 4×4 matrix that represents the equivalent three-phase source impedance seen by a group of three PSUs in a power shelf. The matrix will be denoted as $\boldsymbol{Z}_{\rm s}(s)$ hereafter. In the following, we assume this matrix has been obtained. Subsection IV.B gives a numerical example to show how this impedance matrix looks.

Note that the distribution network involves several different voltages. Obviously, the impedances of different segments must be converted to the same voltage level before they can be combined with other segments in the scaling. Here we assume all impedances are referred to the voltage at the PSU input terminal. An additional factor to consider in a Y-configured system is the starting point of the neutral. As mentioned before, the neutral is usually provided on the secondary of the distribution transformer (PTX in Fig. 1). To account for this partial neutral path, each impedance above the PTX can still be expressed by a 4×4 matrix but with the elements related to the neutral (both self and mutual impedance) set to zero.

The equivalent circuit in Fig. 3 did not explicitly include the coupled current responses of the PSU that we modeled in Part I. However, it is easy to see that, under the assumptions stated at the beginning of this subsection, the equivalent source impedance defined by (6) (and its matrix version) is also valid when coupled current responses are considered.

III. Three-Phase System Modeling and Stability

The equivalent source impedance defined in the last section allows us to study the stability of a data center power system using a simplified model involving just three PSUs. The objective of this section is to model such a three-PSU system. This is usually a straightforward process, but is complicated here because of the need to:

- Eliminate the redundancy in the model caused by coupling among three phases; and
- Include the coupled current responses.

We will develop the desired system model step-by-step in the following subsections. Since the modeling of Y-connected PSUs with neutral is more complex and has the additional zero-sequence to be considered, we will focus on it in this section. Fig. 4 shows the equivalent three-PSU system that will be modeled. Modeling of Δ-connected systems will be discussed in Subsection IV.D.

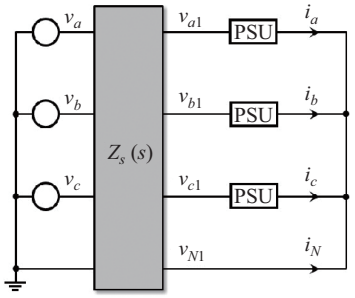

Fig. 4. A reduced system model representing a data center power system that uses Y-connected PSUs.

A. Equivalent Circuits with Coupled Current

Similar to the single-converter system modeled in Part I, the response of the three-PSU system in Fig. 4 to a voltage perturbation at frequency s in the source voltage can be represented by the two equivalent circuits given in Fig. 5. The circuits are essentially obtained by duplicating the single-PSU models used in [1] for each PSU. All variables used in the circuits are considered small-signal variables. However, to simplify the notation, the hat used in (1)–(3) to signify a small-signal variable is dropped. As indicated before, the

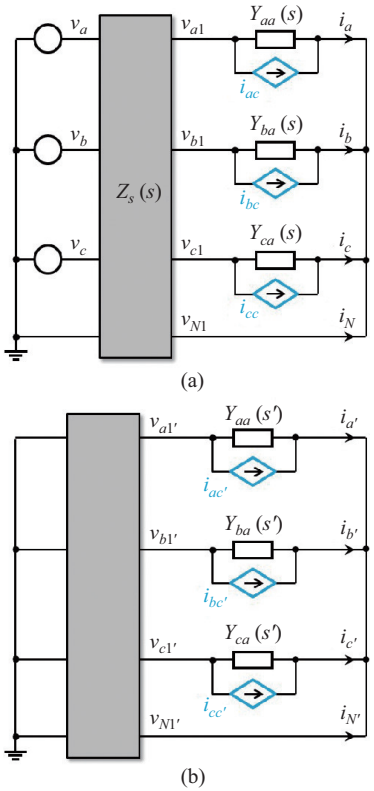

Fig. 5. Frequency-domain models of the circuit in Fig. 4; (a) the perturbation frequency, and b) the coupling frequency.

second coupled current at frequency $s+j2\omega_1$ is much smaller than the one at $s-j2\omega_1$, hence will be ignored in the system model.

Figure 5(a) is the equivalent circuit at the perturbation frequency. It involves the PSU input admittance $Y_{\rm a}$ as well as the equivalent grid impedance $\boldsymbol{Z}_{\rm s}$ at frequency s. The three voltage sources behind the equivalent source impedance represent the applied voltage perturbation. Fig. 5(b) is the equivalent circuit at the coupling frequency ($s-j2\omega_1$) and involves the PSU input admittance $Y_{\rm a}$ as well as the equivalent grid impedance $\boldsymbol{Z}_{\rm s}$ at the coupling frequency. To shorten the expressions, the coupling frequency will be denoted as s', that is, $s'=s-j2\omega_1$. There is no voltage source in Fig. 5(b) because no external perturbation is applied at $s-j2\omega_1$.

As in the single-phase case presented in Part I, each of the controlled current sources in Fig. 5(a) and 5(b) models a coupling between the response of a PSU at the perturbation and the coupling frequency. Each such current source in Fig. 5(a) depends on the voltage across the PSU terminals (between the phase and neutral) in Fig. 5(b) and represents the coupled current at frequency s produced by the induced voltage perturbation at $s-j2\omega_1$. Likewise, each controlled current source in Fig. 5(b) depends on the voltage across the PSU terminals in Fig. 5(a) and represents the coupled current at frequency $s-j2\omega_1$ produced by the voltage at frequency s.

B. Three-Phase System Model

As the next step, we will model the two equivalent circuits in Fig. 5 to find the total current responses of the three PSUs at the perturbation frequency. Since the three PSUs operate with balanced input voltages and are supposed to supply equal power to *their loads*, their impedance models should be the same. However, to provide a more general formulation, we assume that the models of the three PSUs can be different, and use an additional letter (a,b,c) in the subscript of each transfer functions defined by (1)–(3) to indicate the phase to which the PSU is connected. For example, $Y_{\rm aa}(s)$, $Y_{\rm ba}(s)$ and $Y_{\rm ca}(s)$ each denotes the input admittance $Y_{\rm a}(s)$ of the PSU connected to phase a, b, and c, respectively. Based on this notation, the following diagonal matrices are also defined to represent the admittances and transfer admittances of the three PSUs together:

$$\boldsymbol{Y}_{\rm a}(s)=\begin{bmatrix} Y_{\rm aa}(s) & 0 & 0\\ 0 & Y_{\rm ba}(s) & 0\\ 0 & 0 & Y_{\rm ca}(s)\end{bmatrix} \tag{7}$$

$$\boldsymbol{Y}_{c-2}(s)=\begin{bmatrix} Y_{{\rm ac}-2}(s) & 0 & 0\\ 0 & Y_{{\rm bc}-2}(s) & 0\\ 0 & 0 & Y_{{\rm cc}-2}(s)\end{bmatrix} \tag{8}$$

$$\boldsymbol{Y}_{c+2}(s)=\begin{bmatrix} Y_{{\rm ac}+2}(s) & 0 & 0\\ 0 & Y_{{\rm bc}+2}(s) & 0\\ 0 & 0 & Y_{{\rm cc}+2}(s)\end{bmatrix} \tag{9}$$

Based on (9) and the relationship among different variables defined in Fig. 5, we can express the three controlled current sources in Fig. 5(a) by voltages of the circuit of Fig. 5(b) in a matrix form as

$$\begin{bmatrix} i_{\rm ac}(s)\\ i_{\rm bc}(s)\\ i_{\rm cc}(s)\end{bmatrix}=\boldsymbol{Y}_{c+2}(s')\begin{bmatrix} v_{a1'}(s')-v_{N1'}(s')\\ v_{b1'}(s')-v_{N1'}(s')\\ v_{c1'}(s')-v_{N1'}(s')\end{bmatrix} \tag{10}$$

Similarly, the three controlled current sources in Fig. 5(b) can be expressed by voltages of the circuit of Fig. 5(a) in a matrix form as

$$\begin{bmatrix} i_{\rm ac'}(s')\\ i_{\rm bc'}(s')\\ i_{\rm cc'}(s')\end{bmatrix}=\boldsymbol{Y}_{c-2}(s)\begin{bmatrix} v_{a1}(s)-v_{\rm N1}(s)\\ v_{b1}(s)-v_{\rm N1}(s)\\ v_{c1}(s)-v_{\rm N1}(s)\end{bmatrix} \tag{11}$$

With the ground reference point placed at the neutral on the source side, the distribution network at the perturbation frequency can be described by the following equation where $\boldsymbol{Z}_{\rm s}(s)$ is the equivalent source impedance:

$$\begin{bmatrix} v_{a1}(s)\\ v_{b1}(s)\\ v_{c1}(s)\\ v_{\rm N1}(s)\end{bmatrix}=\begin{bmatrix} v_{\rm a}(s)\\ v_{\rm b}(s)\\ v_{\rm c}(s)\\ 0\end{bmatrix}-\boldsymbol{Z}_{\rm s}(s)\begin{bmatrix} i_{\rm a}(s)\\ i_{\rm b}(s)\\ i_{\rm c}(s)\\ i_{\rm N}(s)\end{bmatrix} \tag{12}$$

The equivalent source impedance $\boldsymbol{Z}_{\rm s}$ is a 4×4 matrix that models the self and mutual impedance of the three phases and the neutral. The neutral current is a dependent variable, hence should be eliminated. We present here a systematic method to achieve that by first defining a matrix

$$\boldsymbol{T}_Y=\begin{bmatrix} 1 & 0 & 0 & -1\\ 0 & 1 & 0 & -1\\ 0 & 0 & 1 & -1\\ 0 & 0 & 0 & 1\end{bmatrix} \tag{13}$$

Multiplying both sides of (12) by this matrix and noting that $i_{\rm N}=-(i_{\rm a}+i_{\rm b}+i_{\rm c})$, we have

$$\begin{bmatrix} v_{a1}(s)-v_{\rm N1}(s)\\ v_{b1}(s)-v_{\rm N1}(s)\\ v_{c1}(s)-v_{\rm N1}(s)\\ v_{\rm N1}(s)\end{bmatrix}=\begin{bmatrix} v_{\rm a}(s)\\ v_{\rm b}(s)\\ v_{\rm c}(s)\\ 0\end{bmatrix}-\boldsymbol{T}_Y\boldsymbol{Z}_{\rm s}(s)\boldsymbol{T}_Y^{\rm T}\begin{bmatrix} i_{\rm a}(s)\\ i_{\rm b}(s)\\ i_{\rm c}(s)\\ 0\end{bmatrix} \tag{14}$$

Note that the neutral current is removed in (14). The last row defines the response of the neutral voltage at the PSU terminal, which is also a dependent variable. To remove this unnecessary equation, define $\boldsymbol{Z}_{\rm s3}(s)$ to represent the upper-left 3×3 block of the matrix $\boldsymbol{T}_Y\boldsymbol{Z}_{\rm s}(s)\boldsymbol{T}_Y^{\rm T}$ and denote the three elements below the block as $Z_{\rm na}(s)$, $Z_{\rm nb}(s)$ and $Z_{\rm nc}(s)$, respectively:

$$\boldsymbol{T}_Y\boldsymbol{Z}_{\rm s}(s)\boldsymbol{T}_Y^{\rm T}=\begin{bmatrix} & \boldsymbol{Z}_{\rm s3}(s) & & \vdots\\ Z_{\rm na}(s) & Z_{\rm nb}(s) & Z_{\rm nc}(s) & \cdot\end{bmatrix} \tag{15}$$

The 4×4 network model (12) can now be replaced by a 3×3 matrix equation between the three phase voltages and currents to exclude the dependent neutral current and voltage:

$$\begin{bmatrix} v_{a1}(s)-v_{\rm N1}(s)\\ v_{b1}(s)-v_{\rm N1}(s)\\ v_{c1}(s)-v_{\rm N1}(s)\end{bmatrix}+\boldsymbol{Z}_{\rm s3}(s)\begin{bmatrix} i_{\rm a}(s)\\ i_{\rm b}(s)\\ i_{\rm c}(s)\end{bmatrix}=\begin{bmatrix} v_{\rm a}(s)\\ v_{\rm b}(s)\\ v_{\rm c}(s)\end{bmatrix} \tag{16}$$

Similarly, the network model at the coupling frequency $s' = s - j2\omega_1$ can be reduced to the following:

$$\begin{bmatrix} v_{a1'}(s') - v_{N1'}(s') \\ v_{b1'}(s') - v_{N1'}(s') \\ v_{c1'}(s') - v_{N1'}(s') \end{bmatrix} + \boldsymbol{Z}_{\mathrm{s3}}(s') \begin{bmatrix} i_{a'}(s') \\ i_{b'}(s') \\ i_{c'}(s') \end{bmatrix} = 0 \tag{17}$$

Equations (10), (11), (16) and (17) can be combined. The result is a model that relates the applied voltage perturbation to the induced current response

$$\begin{bmatrix} i_{\mathrm{a}}(s) \\ i_{\mathrm{b}}(s) \\ i_{\mathrm{c}}(s) \end{bmatrix} = \{\boldsymbol{I} + \boldsymbol{Y}_l(s)\boldsymbol{Z}_{\mathrm{s3}}(s)\}^{-1} \cdot \boldsymbol{Y}_l(s) \begin{bmatrix} v_{\mathrm{a}}(s) \\ v_{\mathrm{b}}(s) \\ v_{\mathrm{c}}(s) \end{bmatrix} \tag{18}$$

where

$$\boldsymbol{Y}_l(s) = \boldsymbol{Y}_{\mathrm{a}}(s) + \boldsymbol{Y}_{\mathrm{l-}}(s) \tag{19}$$

$$\boldsymbol{Y}_{\mathrm{l-}}(s) = -\boldsymbol{Y}_{c+2}(s') \left[\boldsymbol{Z}_{\mathrm{s3}}^{-1}(s') + \boldsymbol{Y}_{\mathrm{a}}(s')\right]^{-1} \boldsymbol{Y}_{c-2}(s) \tag{20}$$

This concludes the first step of the first objective defined in the Introduction. The admittance matrix (20) is a generalization to the function $Y_{\mathrm{l-}}(s)$ defined by Eq. (36) of Part I for a single-converter system. This added term is only necessary for system stability analysis below the second harmonic frequency. Above that, the coupled current can be ignored, such that $\boldsymbol{Y}_{\mathrm{l-}}(s)$ can be set to zero and $\boldsymbol{Y}_l(s)$ simplifies to $\boldsymbol{Y}_{\mathrm{a}}(s)$.

C. Stability

Our goal is to develop a mathematical model that can be used to determine the stability of the three-PSU system defined in Fig. 4. To that end, note that the impedance-based matrix model (18) is the same as the closed-loop transfer function of the three-input three-output (3I3O) feedback system depicted in Fig. 6, with $\boldsymbol{Y}_l(s)$ as the forward matrix and $\boldsymbol{Z}_{\mathrm{s3}}(s)$ the feedback matrix. Accordingly, stability of the three-PSU system is the same as the stability of the feedback system, in other words, stability of the loop transfer matrix:

$$\boldsymbol{L}(s) = \boldsymbol{Y}_l(s)\boldsymbol{Z}_{\mathrm{s3}}(s) \tag{21}$$

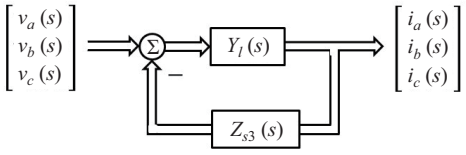

Fig. 6. Representation of three-phase impedance model (18) as a 3I3O feedback control system.

Since the three-PSU system is equivalent to the original data center power system in terms of stability, (21) also represents the stability of the data center power system.

MIMO system stability can be assessed by the generalized Nyquist criterion (GNC). While there are several variations, the basic form of the GNC is to apply the Nyquist criterion to the determinant of the return difference matrix $\boldsymbol{I} + \boldsymbol{L}(s)$ or the eigenvalue (characteristic) loci of the loop transfer matrix $\boldsymbol{L}(s)$ [24]. Since both the determinant and the eigenvalues are complex functions of the loop transfer matrix, stability analysis usually has to be performed numerically, making it difficult to gain insights and develop general conclusions. We will avoid this difficulty in the next section by converting the 3I3O model (18) into three separate SISO models using sequence impedances. Here we take a closer look at (21) to understand its complexity and point out some special cases that may allow (21) to be simplified without using sequence impedances.

Assuming that the three phases of the distribution system are symmetrical, we can write the equivalent source impedance matrix $\boldsymbol{Z}_{\mathrm{s}}$ as follows (without the frequency variable s to shorten the expression) where Z_{p} is the self-impedance of each phase, Z_{n} is the self-impedance of the neutral, Z_{pp} is the mutual impedance between phases, and Z_{pn} is the mutual impedance between each phase and the neutral:

$$\boldsymbol{Z}_{\mathrm{s}} = \begin{bmatrix} Z_{\mathrm{p}} & Z_{\mathrm{pp}} & Z_{\mathrm{pp}} & Z_{\mathrm{pn}} \\ Z_{\mathrm{pp}} & Z_{\mathrm{p}} & Z_{\mathrm{pp}} & Z_{\mathrm{pn}} \\ Z_{\mathrm{pp}} & Z_{\mathrm{pp}} & Z_{\mathrm{p}} & Z_{\mathrm{pn}} \\ Z_{\mathrm{pn}} & Z_{\mathrm{pn}} & Z_{\mathrm{pn}} & Z_{\mathrm{n}} \end{bmatrix} \tag{22}$$

The neutral carries less (ideally no) current, hence may be sized differently. As discussed early in this section, neutral connection also does not go all the way to the grid. For these reasons, the neutral self- and mutual impedances in (22) are assumed to be different from the phase impedances. Based on the definition given in (15), the equivalent three-phase source impedance in this case is a symmetrical matrix given below where the diagonal elements are $Z_{\mathrm{d}} = Z_{\mathrm{p}} + Z_{\mathrm{n}} - 2Z_{\mathrm{pn}}$ and off-diagonal elements are $Z_{\mathrm{m}} = Z_{\mathrm{n}} + Z_{\mathrm{pp}} - 2Z_{\mathrm{pn}}$:

$$\boldsymbol{Z}_{\mathrm{s3}} = \begin{bmatrix} Z_{\mathrm{d}} & Z_{\mathrm{m}} & Z_{\mathrm{m}} \\ Z_{\mathrm{m}} & Z_{\mathrm{d}} & Z_{\mathrm{m}} \\ Z_{\mathrm{m}} & Z_{\mathrm{m}} & Z_{\mathrm{d}} \end{bmatrix} \tag{23}$$

Note that both $\boldsymbol{Z}_{\mathrm{s}}$ and $\boldsymbol{Z}_{\mathrm{s3}}$ are symmetrical matrices. The diagonal elements of $\boldsymbol{Z}_{\mathrm{s3}}$ are also identical. The off-diagonal elements depend on the neutral self-impedance as well as both mutual impedances Z_{pp} and Z_{pn}. With this source impedance, $\boldsymbol{Y}_{\mathrm{l-}}(s)$ is a full matrix (with non-zero off-diagonal elements), making $\boldsymbol{L}(s)$ a full and complex matrix in general. Therefore, the generalized Nyquist criterion is required to determine stability.

In some special cases, the off-diagonal elements of $\boldsymbol{Z}_{\mathrm{s3}}$ may be small and negligible. For example, if the neutral is created at location close to the PSUs, the neutral connection may be very short such that $Z_{\mathrm{n}} \approx 0, Z_{\mathrm{pn}} \approx 0$. Additionally, the mutual impedance Z_{pp} among the phases may be small and negligible if the phase conductors are laid out with sufficient distance between each other. Under these conditions, $\boldsymbol{Z}_{\mathrm{s3}}$ reduces to a scalar matrix and $Z_{\mathrm{d}}(s) = Z_{\mathrm{p}}(s)$. Furthermore, assume that the three PSUs are identical such that $\boldsymbol{Y}_{\mathrm{a}}(s)$, $\boldsymbol{Y}_{c-2}(s)$ and $\boldsymbol{Y}_{c+2}(s)$ are all scalar matrices. This also causes $\boldsymbol{Y}_l(s)$ to be a scalar matrix, that is, $\boldsymbol{Y}_l(s) = \mathrm{diag}\left[\{Y_l(s), Y_l(s), Y_l(s)\}\right]$ where

$$Y_l(s) = Y_{\mathrm{a}}(s) - \frac{Y_{c+2}(s - j2\omega_1)Y_{c-2}(s)}{Y_{\mathrm{a}}(s - j2\omega_1) + Z_{\mathrm{p}}^{-1}(s - j2\omega_1)} \tag{24}$$

Note (24) is the same as the input admittance calculated in Part I for a single PSU connected to a grid with source

impedance $Z_{\rm p}(s)$. With these, the loop transfer matrix (21) becomes

$$\boldsymbol{L}(s)=\begin{bmatrix} Y_l(s)Z_{\rm p}(s) & 0 & 0\\ 0 & Y_l(s)Z_{\rm p}(s) & 0\\ 0 & 0 & Y_l(s)Z_{\rm p}(s)\end{bmatrix} \tag{25}$$

Since $\boldsymbol{L}(s)$ is diagonal, the diagonal elements are also its eigenvalues. Therefore, stability of the three-PSU system in this case can be determined by applying the Nyquist criterion to $Y_l(s)Z_{\rm p}(s)$. In other words, the system has the same stability as one PSU connected to a source with impedance $Z_{\rm p}(s)$. This is expected because the three PSUs operate independently when there is no phase coupling and no neutral impedance.

Another special case in which application of the generalized Nyquist criterion can be simplified is system stability in the medium- and high-frequency range where $\boldsymbol{Y}_{\rm l-}(s)$ can be ignored. (Recall the definition of different frequency ranges in Part I.) Since $\boldsymbol{Y}_l(s)=\boldsymbol{Y}_{\rm a}(s)$ becomes a scalar matrix, the eigenvalues of $\boldsymbol{L}(s)$ can be obtained by multiplying each of the eigenvalues of $\boldsymbol{Z}_{\rm s3}(s)$ by $Y_{\rm a}(s)$. Based on (23), the eigenvalues of $\boldsymbol{Z}_{\rm s3}(s)$ are:

$$\lambda_1(s)=\lambda_2(s)=Z_{\rm p}(s)+Z_{\rm pp}(s) \tag{26}$$

$$\lambda_3(s)=Z_{\rm p}(s)+3Z_{\rm n}(s)+3Z_{\rm pp}(s)-6Z_{\rm pn}(s) \tag{27}$$

Therefore, stability of the system in this case can be determined by applying the Nyquist criterion to each of the following frequency-domain models:

$$l_1(s)=l_2(s)=Y_{\rm a}(s)\left[Z_{\rm p}(s)+Z_{\rm pp}(s)\right] \tag{28}$$

$$l_3(s)=Y_{\rm a}(s)\left[Z_{\rm p}(s)+3Z_{\rm m}(s)\right] \tag{29}$$

As can be seen, there are special cases in which the 3I3O system model (21) can be decomposed into separate SISO models to avoid the need for the GNC. However, simplification of the system model in these special cases involve assumptions that do not hold in general and require ad hoc methods to decompose the model.

IV. Stability Analysis in the Sequence Domain

Symmetrical component analysis of three-phase systems is based on decomposing each phase variable in a three-phase system into a zero, a positive, and a negative sequence component. The transformation from phase to symmetrical components uses the matrix $\boldsymbol{S}$ defined below:

$$\boldsymbol{S}=\frac{1}{3}\begin{bmatrix}1 & 1 & 1\\ 1 & \boldsymbol{a} & \boldsymbol{a}^2\\ 1 & \boldsymbol{a}^2 & \boldsymbol{a}^2\end{bmatrix},\ \boldsymbol{a}=e^{j\frac{2\pi}{3}}=-\frac{1}{2}+j\frac{\sqrt{3}}{2} \tag{30}$$

In this work, a zero, positive and negative sequence component will be denoted by a number 0, 1 and 2 in the subscript, respectively. In a vector form, the three sequence components are defined as follows:

$$\begin{bmatrix}v_0(s)\\ v_1(s)\\ v_2(s)\end{bmatrix}=\boldsymbol{S}\begin{bmatrix}v_{\rm a}(s)\\ v_{\rm b}(s)\\ v_{\rm c}(s)\end{bmatrix},\ \begin{bmatrix}i_0(s)\\ i_1(s)\\ i_2(s)\end{bmatrix}=\boldsymbol{S}\begin{bmatrix}i_{\rm a}(s)\\ i_{\rm b}(s)\\ i_{\rm c}(s)\end{bmatrix} \tag{31}$$

Based on this notation, the three-PSU system model (18) can be transformed into the sequence domain as

$$\begin{bmatrix}i_0(s)\\ i_1(s)\\ i_2(s)\end{bmatrix}=\{\boldsymbol{I}+\boldsymbol{Y}_{\rm l012}(s)\boldsymbol{Z}_{\rm s012}(s)\}^{-1}\boldsymbol{Y}_{e012}(s)\begin{bmatrix}v_0(s)\\ v_1(s)\\ v_2(s)\end{bmatrix} \tag{32}$$

where

$$\boldsymbol{Y}_{\rm l012}(s)=\boldsymbol{S}\boldsymbol{Y}_l(s)\boldsymbol{S}^{-1} \tag{33}$$

$$\boldsymbol{Z}_{\rm s012}(s)=\boldsymbol{S}\boldsymbol{Z}_{\rm s3}(s)\boldsymbol{S}^{-1} \tag{34}$$

The sequence-domain model (32) is in the same form as the three-phase model (18) and can be represented by a 3I3O feedback system, similar to that in Fig. 6, with their loop transfer matrices related to each other by

$$\boldsymbol{L}_{\rm s012}(s)=\boldsymbol{S}\boldsymbol{L}(s)\boldsymbol{S}^{-1} \tag{35}$$

Since $\boldsymbol{S}$ is invertible, the two matrices in (35) are similar, hence have the same eigenvalues [25]. Therefore, (32) can be used in place of (18) for stability study of the three-PSU system.

It is also worth noting that the sequence transformation is exchangeable with scaling according to (6). Based on that, the impedance of each component/segment of the network can be converted to the sequence domain and then used in (6) to define the equivalent sequence impedance $\boldsymbol{Z}_{\rm s012}$.

A. Balanced System Stability Analysis

With the assumed symmetry in $\boldsymbol{Z}_{\rm s}$ as indicated in (22), the sequence impedance matrix $\boldsymbol{Z}_{\rm s012}(s)$ is diagonal,

$$\boldsymbol{Z}_{\rm s012}=\begin{bmatrix}Z_{\rm s0}(s) & 0 & 0\\ 0 & Z_{\rm s1}(s) & 0\\ 0 & 0 & Z_{\rm s2}(s)\end{bmatrix} \tag{36}$$

where $Z_{\rm s0}(s)$, $Z_{\rm s1}(s)$ and $Z_{\rm s2}(s)$ is the ESI in the zero, positive and negative sequence, respectively:

$$Z_{\rm s0}(s)=Z_{\rm p}(s)+3Z_{\rm n}(s)+2Z_{\rm pp}(s)-6Z_{\rm pn}(s)$$

$$Z_{\rm s1}(s)=Z_{\rm s2}(s)=Z_{\rm p}(s)+Z_{\rm pp}(s)$$

Similarly, with three identical PSUs and symmetrical $\boldsymbol{Z}_{\rm s}$, $\boldsymbol{Y}_{\rm l012}(s)$ also becomes diagonal,

$$\boldsymbol{Y}_{\rm l012}(s)=\begin{bmatrix}Y_{\rm l0}(s) & 0 & 0\\ 0 & Y_{\rm l1}(s) & 0\\ 0 & 0 & Y_{\rm l2}(s)\end{bmatrix} \tag{37}$$

where

$$Y_{\rm l0}(s)=Y_{\rm a}(s)-\frac{Y_{c+2}(s-j2\omega_1)Y_{c-2}(s)}{Y_{\rm a}(s-j2\omega_1)+Z_{\rm s0}^{-1}(s-j2\omega_1)} \tag{38}$$

$$Y_{\rm l1}(s)=Y_{\rm a}(s)-\frac{Y_{c+2}(s-j2\omega_1)Y_{c-2}(s)}{Y_{\rm a}(s-j2\omega_1)+Z_{\rm s1}^{-1}(s-j2\omega_1)} \tag{39}$$

$$Y_{\rm l2}(s)=Y_{\rm a}(s)-\frac{Y_{c+2}(s-j2\omega_1)Y_{c-2}(s)}{Y_{\rm a}(s-j2\omega_1)+Z_{\rm s2}^{-1}(s-j2\omega_1)} \tag{40}$$

The sequence impedance and admittance matrices $\boldsymbol{Z}_{\mathrm{s}012}$ and $\boldsymbol{Y}_{\mathrm{l}012}(s)$ are diagonal even when $\boldsymbol{Z}_{\mathrm{s}}$ is "less symmetrical" than indicated in (22). For example, with

$$\boldsymbol{Z}_{\mathrm{s}} = \begin{bmatrix} Z_{\mathrm{p}} & Z_{m^+} & Z_{m^-} & Z_{\mathrm{pn}} \\ Z_{m^-} & Z_{\mathrm{p}} & Z_{m^+} & Z_{\mathrm{pn}} \\ Z_{m^+} & Z_{m^-} & Z_{\mathrm{p}} & Z_{\mathrm{pn}} \\ Z_{\mathrm{pn}} & Z_{\mathrm{pn}} & Z_{\mathrm{pn}} & Z_{\mathrm{n}} \end{bmatrix} \tag{41}$$

matrix $\boldsymbol{Z}_{\mathrm{s}012}$ assumes the same diagonal form as in (36), with each of the sequence impedances defined as follows:

$$\begin{aligned} Z_{\mathrm{s}0}(s) &= Z_{\mathrm{p}}(s) + 3Z_{\mathrm{n}}(s) \\ &\quad + Z_{m^+}(s) + Z_{m^-}(s) - 6Z_{\mathrm{pn}}(s) \end{aligned} \tag{42}$$

$$Z_{\mathrm{s}1}(s) = Z_{\mathrm{p}}(s) + \boldsymbol{a}^2 Z_{m^+}(s) + \boldsymbol{a} Z_{m^-}(s) \tag{43}$$

$$Z_{\mathrm{s}2}(s) = Z_{\mathrm{p}}(s) + \boldsymbol{a} Z_{m^+}(s) + \boldsymbol{a}^2 Z_{m^-}(s) \tag{44}$$

Sequence admittance models (38)–(40) can still be used to the model the PSUs in this more general case; the only change required is to replace $Z_{\mathrm{s}0}(s)$, $Z_{\mathrm{s}1}(s)$ and $Z_{\mathrm{s}2}(s)$ by (42)–(44). Compared to (22), the "less symmetrical" $\boldsymbol{Z}_{\mathrm{s}}$ (41) causes the positive- and negative-sequence impedance to be different. This property is useful for the modeling of certain three-phase components such as backup generators, hence will be assumed in the rest of the work.

With both $\boldsymbol{Z}_{\mathrm{l}012}(s)$ and $\boldsymbol{Y}_{\mathrm{l}012}(s)$ in a diagonal form, (32) can be broken down into three separate models:

$$i_0(s) = \left[1 + Y_{\mathrm{l}0}(s) Z_{\mathrm{s}0}(s)\right]^{-1} Y_{\mathrm{l}0}(s) v_0(s) \tag{45}$$

$$i_1(s) = \left[1 + Y_{\mathrm{l}1}(s) Z_{\mathrm{s}1}(s)\right]^{-1} Y_{\mathrm{l}1}(s) v_1(s) \tag{46}$$

$$i_2(s) = \left[1 + Y_{\mathrm{l}2}(s) Z_{\mathrm{s}2}(s)\right]^{-1} Y_{\mathrm{l}2}(s) v_2(s) \tag{47}$$

Each of (45)–(47) can be interpreted as an SISO feedback system representing the three-PSU system in the zero, positive and negative sequence, respectively. Stability of each SISO model can be determined by applying the Nyquist criterion to the corresponding loop gain $Y_{\mathrm{lk}}(s) Z_{\mathrm{sk}}(s), k = 0, 1, 2$. The three-PSU system is stable if and only if all three SISO models (45)–(47) are stable, in other words, if it is stable in each of the three sequences.

The development presented above is an extension to the existing small-signal sequence impedance theory for three-phase converter systems [23]. Compared to wind, PV, HVDC and other systems that are based on three-phase converters, the application in data centers requires:

- Formulation of sequence impedance models from single-phase converter models instead of directly developing them for three-phase converters
- Inclusion of the zero sequence as part of the system model

B. Zero-Sequence Stability and Low Frequency Resonance

The SISO models (45)–(47) reduce the stability analysis of a data center power system to that of a single PSU operating with different source impedance. This allows us to relate the overall data center stability to the analyses and findings presented in Part I [1] for a single-PSU system. The following modes of instability were identified in Part I for a single PSU:

- *Low Frequency*: Below the second harmonic frequency, DC bus voltage control causes the PSU input impedance to dip at two frequency points that are symmetrical about the fundamental, as well as to be negatively damped between the two points. The dipping makes the PSU impedance more likely to intersect with the source impedance and develop an unstable resonance. Through the coupled current, a high source impedance also has the effect to increase the dipping in the PSU impedance, making it more likely to intersect with the source impedance. Therefore, the higher the source impedance is, the more likely the PSU may become unstable in the low-frequency range.
- *High Frequency*: Digital control and PWM delay leads to negative damping at high frequency. This makes it possible for the PSU to develop instability and resonance in the high-frequency range with either the passive distribution network or a UPS.

To see how these modes may play out in a data center power system, we need to characterize the equivalent source impedance used in (45)–(47) more quantitatively. To that end, the Meta engineering team has measured the impedance of different components used in Meta data centers. Finite element simulation was also used to model some of the components to correlate with the measurements and to quantify the characteristics that are difficult to measure directly. For the purpose of this work, we will use an RL circuit to represent each impedance element and ignore possible dependency of the RL values on frequency. With this assumption, each impedance can also be specified by its value at the fundamental frequency.

As an example, following is the equivalent source impedance $\boldsymbol{Z}_{\mathrm{s}}$ at the fundamental frequency (60 Hz) for a notional data center power system:

$$\begin{bmatrix} 2.4 + 24.95i & 0.87 + 4.83i & 0.87 + 4.84i & 0.72 + 3.13i \\ 0.87 + 4.84i & 2.4 + 24.95i & 0.87 + 4.83i & 0.72 + 3.13i \\ 0.87 + 4.83i & 0.87 + 4.84i & 2.4 + 24.95i & 0.72 + 3.13i \\ 0.72 + 3.13i & 0.72 + 3.13i & 0.72 + 3.13i & 2.56 + 7.59i \end{bmatrix} \tag{48}$$

The corresponding 3×3 impedance matrix $\boldsymbol{Z}_{\mathrm{s}3}$ and sequence impedance matrix $\boldsymbol{Z}_{\mathrm{s}012}$ are calculated to be:

$$\boldsymbol{Z}_{\mathrm{s}3}(j\omega_1) = \begin{bmatrix} 3.51 + 26.28i & 1.99 + 6.17i & 1.99 + 6.17i \\ 1.99 + 6.17i & 3.51 + 26.28i & 1.99 + 6.17i \\ 1.99 + 6.17i & 1.99 + 6.167i & 3.51 + 26.28i \end{bmatrix}$$

$$\boldsymbol{Z}_{\mathrm{s}012}(j\omega_1) = \begin{bmatrix} 7.49 + 38.6i & 0 & 0 \\ 0 & 1.52 + 20.11i & 0 \\ 0 & 0 & 1.53 + 20.11i \end{bmatrix}$$

Note that the positive- and negative-sequence impedances are virtually the same in this example. This is because the two mutual impedances Z_{m^+} and Z_{m^-} are almost identical. Since the PSU positive- and negative-sequence impedances $Y_{\mathrm{l}1}$ and $Y_{\mathrm{l}2}$ are equal when the three PSUs are identical and operate under the same condition, stability of the system in these two sequences is also the same.

The first diagonal element of $\boldsymbol{Z}_{\mathrm{s}012}$ is the zero-sequence impedance and is almost two times higher in magnitude then the positive- and negative-sequence impedance. This is because the zero-sequence impedance includes three times the neutral line impedance Z_{n} that does not affect the positive- and

negative-sequence impedance, as can be seen from (32)–(44). According to (38), a high zero-sequence source impedance also increases the zero-sequence admittance of the PSU. The combination of these two factors makes the loop gain of (45) much higher than the other two.

Since the ESI is defined for individual PSUs, it should be evaluated relative to a PSU input impedance. To that end, we define a *base impedance ratio* (BIR) in each of the three sequences as follows:

$$\sigma_k = \frac{Z_{\rm b}}{|Z_{\rm sk}(j\omega_1)|},\ k = 0, 1, 2 \tag{49}$$

$Z_{\rm b}$ is the base impedance of the PSU and is defined as the ratio of the PSU rated voltage ($V_{\rm N}$) to the rated current ($I_{\rm N}$):

$$Z_{\rm b} = \frac{V_{\rm N}}{I_{\rm N}} \tag{50}$$

The BIR is similar to the short circuit ratio (SCR) used in the utility industry. It is given a different name here because there is no measurable short circuit current in a data center that corresponds to the abstract equivalent source impedance.

Applying the definition (49) to a typical 1-kW PSU in a 480 V system ($Z_{\rm b} = 76.8\Omega$) and the example ESI (48), we found

$$\sigma_0 = 1.95, \quad \sigma_1 = 3.81, \quad \sigma_2 = 3.81$$

The low BIR indicates a "soft" source, akin to a weak grid for a wind and PV farm. In particular, $\sigma_0 = 1.95$ indicates that the PSU impedance is only about ($20\log_{10} 1.95 \approx$) 6 dB above the equivalent source impedance near the fundamental frequency in the zero sequence. The analyses in Part I have shown that the PSU input impedance may dip 10 dB or more near the fundamental frequency and the dipping may be further increased by another 10 dB when the source impedance is high. This, coupled with the negative damping in the PSU impedance, explains the low frequency resonances observed in Meta data centers, as described in Part I of the work [1].

The fact that the BIR is the lowest in the zero sequence also implies that *zero sequence is the weakest link and the first one to become unstable in a data center power system that uses Y-connected PSUs*. Instability in the zero sequence will manifest itself as growing or sustained harmonics at the resonance frequency that form a zero sequence, in other words, they are the same among the three phases. This will be confirmed by the laboratory and actual data center measurements presented in Section VI.

The low BIR also implies that PSUs will unlikely develop high frequency resonances in the path that is modeled by the equivalent source impedance. As discussed in Part I and summarized early, control delay and the associated negative damping is the root cause for high frequency resonance. For a typical PSU design, the negative damping starts from several kHz. With a low-BIR source, the inductive ESI would be 30–40 dB above the PSU base impedance in that frequency range. In contrast, the PSU input impedance at high frequency is dominated by the filter capacitors and will not be much higher than the base impedance at its peaking point [1]. Therefore, with a low BIR, the ESI and the PSU input impedance usually will not intersect again above the second harmonic frequency; hence will not form a resonance in the high-frequency range. The expanded system model presented in Section V will explain how PSUs may develop high frequency resonance with the passive distribution system.

The discussion so far has been directed to PSUs supplied directly from the grid. The developed method can also be used to study the stability of PSUs supplied from a UPS. To do that, the scaling method can be applied to the UPS output impedance and the impedance of the distribution network between the UPS and the PSU to redefine the equivalent source impedance. The system models remain the same as developed in this and last section, and can be broken down into zero-, positive- and negative-sequence models as in (45)–(47). However, with a UPS as the source, the equivalent source impedance is significantly different from that of a passive distribution network, leading to different system behavior and stability characteristics:

- Because of the low output impedance of the UPS and the short distance from a UPS to the PSUs, the BIR is usually much higher than that for PSUs powered directly from the grid. Therefore, low frequency resonance is much less likely for PSUs powered from a UPS. An exception is the UPS operating in bypass mode, in which case the UPS merely adds an impedance to the ESI through the bypass.
- The UPS output impedance at high frequency is also dominated by its output filter and may be negatively damped because of its own control delay. This makes it possible for high frequency resonance to develop between PSUs and the UPS. This mode of resonance has been identified in Part I of the work and can be predicted using the method and models presented in this section.

C. Improving Zero-Sequence Stability

The example BIRs calculated in the last subsection are representative of Meta data centers. Actual values vary from site to site and with the voltage level, and could be lower. The low BIR presents a challenge for maintaining stable operation of the data center power system in the low-frequency range, especially in the zero sequence. Negative damping in the PSU input impedance is one of the root causes for instability below the second harmonic frequency but cannot be eliminated, as discussed in Part I of the work. One practical technique to improve low-frequency stability is to minimize the dipping in the magnitude of the PSU input impedance. This can be partially achieved by maintaining a sufficient phase margin in the front-end PFC converter voltage control [1]. Other techniques to optimize PSU design for system stability will be presented in a future work.

Since zero sequence is the weakest link, reducing the equivalent source impedance in the zero sequence has to be an important objective for data center distribution system design. As can be seen from (42)–(44), the zero sequence impedance includes three times the neutral impedance. To minimize this impedance, we recommend the following methods:

- The neutral conductors should be sized properly to keep its self-impedance low. This may require larger conductors than otherwise needed.

- The distribution transformer at which the neutral for the PSU is created should be kept as close to the PSUs as possible.
- Use of other components such as current limiting or harmonic filtering reactors in the neutral should be avoided.

The mutual impedances among the phases and between each phase and the neutral also contribute to the zero-sequence impedance, but have opposite effects: As (42) indicates, the coupling among the phases adds to Z_{s0} while the coupling between phase and neutral reduces Z_{s0}. The reduction effect by phase-neutral coupling can be significant because of the multiplying factor 6. This relationship can be exploited in the cable layout design to reduce Z_{s0} by purposely reducing phase-phase coupling while enhancing phase-neutral coupling. Fig. 7 illustrates the concept, where the layout a) could have significantly less zero-sequence impedance than b).

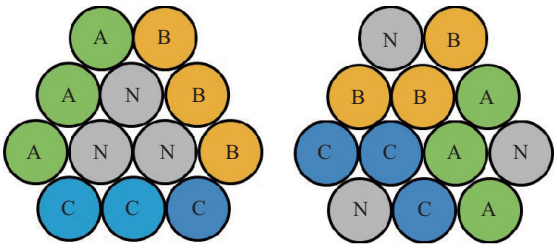

Fig. 7. Cross sectional diagrams showing two different cable layouts for data center power distribution network.

A number of variations based on Fig. 7 may be considered in practical design depending on the number of cables used in each phase and other constraints of the building system. As an example to show the level of improvement achievable by this method, consider the network modeled by (48). The zero-sequence BIR for the 1-kW PSU would increase from 1.95 to 2.64 if the phase-neutral mutual impedance can be made the same as the phase-phase mutual impedance, that is, if each off-diagonal element in the last column and last row of the matrix in (48) can be increased from $0.72 + 3.13i$ to $0.87 + 4.83i$.

It is worth noting from (38)–(40) that the PSU input admittance is the same in positive, negative and zero sequence if coupling through the source impedance is ignored. The high source impedance in the zero sequence will cause the zero-sequence admittance $Y_{l0}(s)$ to peak more at two frequency points near the fundamental, as the analysis in Part I showed. This further increases the potential for instability in the zero sequence. On the other hand, the effects of PSU design, including its control, are the same on all three sequence-admittances of a three-PSU group. Therefore, improvement in PSU input impedance would benefit system stability in all three sequences.

It shall also be pointed out that, while a symmetrical three-phase distribution network has been assumed, the techniques discussed above to reduce zero-sequence impedance of the network would also help to improve system stability when the system is asymmetric.

D. Δ Configuration

The methods presented so far can be extended to PSUs in Δ configuration. The equivalent source impedance is obtained based on (6) but is a 3×3 matrix because there is no neutral. The reduced three-PSU system is also modeled by two equivalent circuits similar that in Fig. 5. The resulting system impedance model is similar to (18) and is given in (52) where

$$\boldsymbol{T}_{\Delta} = \begin{bmatrix} 1 & -1 & 0 \\ 0 & 1 & -1 \\ -1 & 0 & 1 \end{bmatrix}$$

$$\begin{bmatrix} i_0(s) \\ i_1(s) \\ i_2(s) \end{bmatrix} = \{\boldsymbol{I} + \boldsymbol{T}_{\Delta}^{\mathrm{T}} \boldsymbol{Y}_l(s) \boldsymbol{T}_{\Delta} \boldsymbol{Z}_{\mathrm{s}}(s)\}^{-1} \boldsymbol{T}_{\Delta}^{\mathrm{T}} \boldsymbol{Y}_l(s) \boldsymbol{T}_{\Delta} \begin{bmatrix} v_0(s) \\ v_1(s) \\ v_2(s) \end{bmatrix} \tag{51}$$

Symmetrical component transformation is then applied to transform (51) into the sequence domain

$$\begin{bmatrix} 1 & 0 & 0 \\ 0 & 1 + 3Y_{\mathrm{l1}}(s) Z_{\mathrm{s1}}(s) & 0 \\ 0 & 0 & 1 + 3Y_{\mathrm{l2}}(s) Z_{\mathrm{s2}}(s) \end{bmatrix} \begin{bmatrix} i_0(s) \\ i_1(s) \\ i_2(s) \end{bmatrix} = \begin{bmatrix} 0 & 0 & 0 \\ 0 & 3Y_{\mathrm{l1}}(s) & 0 \\ 0 & 0 & 3Y_{\mathrm{l2}}(s) \end{bmatrix} \begin{bmatrix} v_0(s) \\ v_1(s) \\ v_2(s) \end{bmatrix} \tag{52}$$

where $Y_{\mathrm{l1}}(s)$ and $Y_{\mathrm{ls}}(s)$ is the PSU input admittance including the effects of the coupled current, as defined by (39) and (40), and $Z_{\mathrm{s1}}(s)$ and $Z_{\mathrm{s2}}(s)$ are the equivalent source impedance in the positive and negative sequence, as defined below:

$$\boldsymbol{S} \boldsymbol{Z}_{\mathrm{s}}(s) \boldsymbol{S}^{-1} = \begin{bmatrix} Z_{\mathrm{s0}}(s) & 0 & 0 \\ 0 & Z_{\mathrm{s1}}(s) & 0 \\ 0 & 0 & Z_{\mathrm{s2}}(s) \end{bmatrix} \tag{53}$$

The first equation in (52) indicates that the zero-sequence current is zero, as expected from the Δ configuration. Based on that and the diagonal form of the matrices, the 3I3O model can be replaced by two separate SISO models, one in the positive sequence and the other in the negative sequence. System stability can then be assessed by applying the Nyquist criterion to each sequence model.

Since there is no instability in the zero sequence, a Δ-configured system would tend to be more stable. However, to compare the two configurations, one has to consider the different distribution voltages. Since Δ-configured PSUs have to operate with line-line voltages, the distribution voltage is usually lower than that in Y-configured system in order to use the same PSU products. The lower distribution voltage implies higher current. This has the effect to lower the base impedance as well as the base impedance ratio, according to the definitions (49) and (50). The models presented in this paper provide a basis to carry out this comparison for practical design.

V. Two-Line System Model and Stability

The single-ESI model developed and used in the preceding sections assumed the network is symmetrical and loaded evenly by PSUs. Other types of loads have been ignored. In

this section, we present an expanded system model that does not require those assumptions. The objectives are of twofold:

- To provide a general methodology that can be used to model the effects of network asymmetry, uneven loading and other factors that may affect system stability.
- To identify a new mode of instability that can explain the high-frequency resonance described in Part I.

A. Two-Line System Model

The expanded system model is defined in Fig. 8 in the form of an equivalent circuit. It includes two parallel lines each supplying a load represented by its admittance $Y_x(s)$ and $Y_y(s)$, respectively. Each line has its own impedance (Z_1 and Z_2), and share a common path to the voltage source v_s.

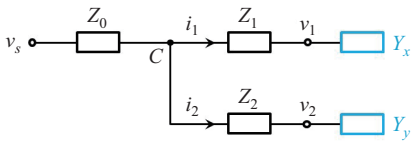

Fig. 8. System model with two parallel branches.

The expanded two-line model may be set up to reflect different non-ideal factors that a single-ESI model cannot capture:

- Network asymmetry, e.g. one MSB is supplied through another MSB under fault. This can be modeled by the circuit with $Z_1 \neq Z_2$, $Y_x = Y_y$.
- Uneven loading, e.g. one MSB or rack is loaded by more PSUs than others are. This can be modeled by the circuit with $Z_1 = Z_2$, $Y_x \neq Y_y$.
- Additional loading by UPS: One of the two loads can represent or include the UPS impedance.

Each line impedance in Fig. 8 can be obtained by applying the scaling method to the corresponding path of the distribution network. To use them together, the scaling must be performed on a common basis. The scaling factors used in (6) are based on the number of PSUs, such that the result is the ESI seen by one PSU. Given the different numbers and types of loads considered in the two-line model, scaling based on power instead of the number of PSUs is more convenient.

The ESI $\boldsymbol{Z}_\mathrm{s}$ used in the last two sections was calculated in three-phase form and then converted to the sequence domain. Since scaling and symmetrical component transformation are both linear operations and exchangeable, we can also model each element of the system by its sequence impedances first and then scale each for use in Fig. 8. Based on this, each impedance in Fig. 8 will be viewed as being already converted to the sequence domain. Since the form of the circuit does not depend on the sequence, we will make no distinction among different sequences in the following discussion except when we want to discuss system behavior in a particular sequence.

A mathematical model for Fig. 8 can be formed in different forms. Our objective is to formulate the model in such a way that conforms to impedance-based stability analysis. To that end, we have developed the model in a matrix form as

$$\begin{bmatrix} i_1(s) \\ i_2(s) \end{bmatrix} = \{\boldsymbol{I} + \boldsymbol{Y}(s)\boldsymbol{Z}(s)\}^{-1}\boldsymbol{Y}(s) \begin{bmatrix} v_\mathrm{s}(s) \\ v_\mathrm{s}(s) \end{bmatrix} \tag{54}$$

where $i_1(s)$ and $i_2(s)$ are the two line currents and the two matrices are defined as follows:

$$\boldsymbol{Y}(s) = \begin{bmatrix} Y_x(s) & 0 \\ 0 & Y_y(s) \end{bmatrix} \tag{55}$$

$$\boldsymbol{Z}(s) = \begin{bmatrix} Z_0(s) + Z_1(s) & Z_0(s) \\ Z_0(s) & Z_0(s) + Z_2(s) \end{bmatrix} \tag{56}$$

Note that $\boldsymbol{Z}(s)$ is symmetrical. The load admittance matrix (55) does not include the coupled current. The coupled-circuit method used in Section III can be applied to develop $\boldsymbol{Y}(s)$ to include such coupling. The result will be similar to (19) and (20), and the final system model (54) will remain the same. Since our focus in this section is to understand the effects of the added complexities and high frequency resonance, we will use the simpler diagonal-form $\boldsymbol{Y}(s)$ as given in (55).

The matrix model (54) can also be generalized to include any number of lines and loads. In fact, the model can be made as granular as having every single PSU, UPS any other load represented separately. This will obviously lead to a very large system model and is not necessary in practice, but is possible. To formulate a model for a system with N loads, one just needs to expand the load admittance $\boldsymbol{Y}(s)$ into a $N \times N$ diagonal matrix to include the admittance of all loads, and formulate the network impedance matrix $\boldsymbol{Z}(s) = [Z_{ij}(s)]_{i,j\in[1,N]}$ as follows:

- $Z_{ii}(s)$ is the sum of impedances of all lines that carry the current of the i^{th} load.
- $Z_{ij}(s)$ is the sum of impedances of all lines that carry the current of both the i^{th} and the j^{th} load.

B. Stability

For stability analysis, note that (54) resembles (18), hence can be treated as the model of a feedback system similar to that shown in Fig. 6, with $\boldsymbol{Y}(s)$ as the forward transfer matrix and $\boldsymbol{Z}(s)$ as the feedback. Based on this, stability of the expanded system model can be determined by applying the GNC to matrix $\boldsymbol{Y}(s)\boldsymbol{Z}(s)$.

Application of the GNC requires quantitative analysis and is only possible when all parameters are given. It is also difficult to define stability margin with GNC. To gain insights and develop general conclusions, we will simplify (54) based on practical system conditions. One approximation we assume is that the two load admittances are proportional to each other and both are derived from a common admittance $Y(s)$:

$$Y_x(s) = N_x Y(s), \quad Y_y(s) = N_y Y(s) \tag{57}$$

This would be the case e.g. when the two lines supply the same type but different number of PSUs. Since modern UPS also uses a PWM rectifier as the front end, its input impedance is similar to PSU input impedance and they share many common features, including dipping in the magnitude and negative damping near the fundamental frequency, as well as negative damping at high frequency due to control delays. Therefore, as an approximation, we can also assume that PSU and UPS input admittances follow the proportionality relationship (57).

With the relationship defined by (57), matrix $\boldsymbol{Y}(s)\boldsymbol{Z}(s)$ can be written as follows:

$$\begin{bmatrix} N_x Z_0(s) + N_x Z_1(s) & N_y Z_0(s) \\ N_x Z_0(s) & N_y Z_0(s) + N_y Z_2(s) \end{bmatrix} Y(s) \quad (58)$$

With a proper selection of $N_x, N_y, Z_1(s)$ and $Z_2(s)$, this model can be set up to represent the different non-ideal factors identified early in the last subsection. To further simplify the analysis, we assume that the line resistance can be ignored such that each line impedance can be represented as an inductor, denoted as $Z_k(s) = sL_k, k = 0, 1, 2$. This allows (58) to be written as follows:

$$\boldsymbol{L}(s) = s \begin{bmatrix} N_x L_0 + N_x L_1 & N_y L_0 \\ N_x L_0 & N_y L_0 + N_y L_2 \end{bmatrix} Y(s) \quad (59)$$

Turn now to the stability of model (54). To apply the GNC, find first the eigenvalues of the inductance matrix in (59). Denoting the eigenvalues as l_1 and l_2, we found:

$$l_1 = \frac{N_x(L_0 + L_1) + N_y(L_0 + L_2)}{2} + \frac{L}{2} \quad (60)$$

$$l_2 = \frac{N_x(L_0 + L_1) + N_y(L_0 + L_2)}{2} - \frac{L}{2} \quad (61)$$

$$L = \sqrt{\begin{matrix}[N_x(L_0 + L_1) + N_y(L_0 + L_2)]^2 \\ -4N_x N_y [L_1 L_2 + L_0(L_1 + L_2)]\end{matrix}} \quad (62)$$

From (59), each eigenvalue of $\boldsymbol{L}(s)$ is an eigenvalue of the inductance matrix multiplied by sY(s):

$$\lambda_1(s) = sl_1 \cdot Y(s), \quad \lambda_2(s) = sl_2 \cdot Y(s) \quad (63)$$

This shows that stability of the two-line system is equivalent to the stability of the two circuits depicted in Fig. 9, where $Y(s)$ represents a load and l_1 and l_2 each represents an equivalent source inductor. Both circuits must be stable in order for the two-line system to be stable. However, since the only difference between the two is the source inductance, we only need to consider the one that is more critical in a given frequency range. Recall also that the two circuits together represent the two-line system in one of the three sequences and should be repeated in other sequence to determine overall stability.

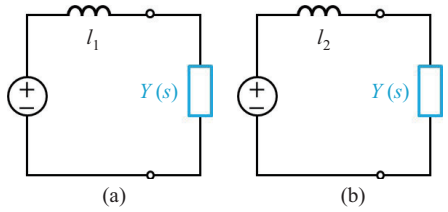

Fig. 9. Equivalent circuits representing the two-line system stability.

With these two equivalent circuits representation of the two-line model, we can now address the two objectives stated at the beginning of this section.

C. Effects of Network Asymmetry and Uneven Loading

Consider stability in the low-frequency range first. Based on Part I and (60)–(63), the circuit in Fig. 9 with higher source inductance (l_1) is more critical. One general question we want to answer is how network asymmetry and uneven loading may change system stability at low frequency. The answer can be developed by comparing the value of l_1 among the four different conditions specified in Table I, where

$$L = \frac{L_1 + L_2}{2}, \quad N = \frac{N_x + N_y}{2} \quad (64)$$

TABLE I
CONDITIONS FOR THE COMPARISON OF l_1

Loading Conditions	Symmetrical Network	Asymmetrical Network
Even Loading	$L_1 = L_2 = L$ $N_x = N_y = N$	$L_2 = 2L - L_1$ $N_x = N_y = N$
Uneven Loading	$L_1 = L_2 = L$ $N_y = 2N - N_x$	$L_2 = 2L - L_1$ $N_y = 2N - N_x$

The comparison is made such that the total load and line impedance are kept constant but distributed differently between the two lines. Based on the definition (60), l_1 is found to assume the smallest value when the network is symmetrical and loaded evenly. This indicates that network asymmetry and uneven loading both tend to make the system less stable at low frequency. Therefore, *to improve data center power system stability at low frequency, the distribution network should be laid out as symmetrically and loaded as evenly as practical.*

As discussed in Section I, AC UPS constitutes a small percentage ($\sim$ 15%) of overall data center loads. The simplified two-line model can also be used to determine the effects of the additional UPS loading on system stability. The model can be set up such that Line 1 includes all PSUs and Line 2 includes all UPS loads. Under the proportionality assumption between PSU and UPS input impedances, a 1-MW UPS would be equivalent to 1000 1 kW PSUs. This provides a practical method to assess the effects of UPS on system stability. It has served as the basis for the development of impedance specifications for UPS that will be discussed in Section VI.

D. DM Stability and High-Frequency Resonance

The smaller eigenvalue l_2 is irrelevant for system stability at low frequency, but its existence signifies a new instability mode that the single-ESI model ignored. To see that, consider first the case of a symmetrical network and even loading. Without losing generality, assume $N_x = N_y = 1$ and $L_2 = L_1$, which reduces (60)–(61) to

$$l_1 = 2L_0 + L_1, \; l_2 = L_1 \quad (65)$$

Based on Fig. 8, l_1 corresponds to the ESI when the two lines are merged together. The corresponding eigenvalue $\lambda_1(s)$ defined in (63) predicts the same instability mode as the single-ESI model would do.

Recall from the definition leading to (59) that L_1 corresponds to the impedance of the line that connects each load to point C where the two lines join. The corresponding eigenvalue is the $\lambda_2(s)$ given in (63). The existence of this eigenvalue in the system stability model indicates that each load may develop instability with the line between the load and point C. This does not seem to make sense at the first glance because they do not form a closed loop to allow a resonance current to circulate. A physically meaningful interpretation is that this

instability mode actually involves the two parallel lines and their loads: It can be seen from Fig. 8 that the two lines do form a loop through the loads, and a current can circulate through one of the phases and the neutral, or in any two of the three sequences. The loop impedance, consisting of two lines and two loads in series, has the same resonance frequency as that of one line with one load. However, this is only the case when the two lines are identical, as assumed in the calculation (65). Without this assumption, l_2 is dependent of L_0 but remains close to the average of L_1 and L_2.

In summary, the expanded two-line system model shows that instability/resonance may also develop between two groups of PSUs or other types of loads through the usually much shorter lines connecting them. For easy reference, we will refer to this mode as a *differential-mode (DM) instability* (*resonance*) and the combined impedance of the two lines as the *equivalent loop impedance (ELI)*.

The DM instability is found to be the root cause for the high frequency resonance described in the Introduction and illustrated in Part I. As pointed out in Subsection IV.B, the high ESI in a typical data center rules out the possibility for high-frequency resonance with the ESI, that, the path that is modeled by the ESI. On the other hand, there are many parallel lines in the radial distribution network. The two-line model can be made to represent such parallel lines at different levels. The corresponding ELI becomes progressively higher as the joint point of the two lines being modeled moves towards the utility side of the network. For example, the ELI between PSU groups within a power shelf or rack is negligibly small, while the ELI between PSUs powered from different substation transformers would be comparable to that of the ESI. With such a wide range of variation, it is likely that the ELI at some level would have the right value to form a resonance with the PSU in the high-frequency range where the PSU input impedance is capacitive because of filter capacitors and is negatively damped because of delay, leading to the observed high frequency resonance.

Relative to the new DM resonance, the low-frequency resonance modeled in the previous sections based on the single-ESI model can be called *common-mode (CM) resonance*. The two types of resonance have several contrasting characteristics beside their different frequencies:A CM resonance would involve all or most loads in the data center; the resulting resonance currents can be measured in all lines, all the way up to the utility grid, and are in phase with each other in parallel lines. On the other hand, a DM resonance would only involve part of the loads, with currents out of phase between lines that form a resonance. Based on this, a low frequency resonance in a data center power system is most likely a CM resonance, while a high frequency resonance that does not involve a UPS is usually a DM resonance. These insights and general understanding make it possible to quickly identify the root cause for practical resonance problems and develop a solution.

VI. Measurements and Impedance-Based Specs

This section presents laboratory and actual data center measurements to support the theory and analyses presented so far. Additional practical issues such as phase unbalance are also discussed. Development of impedance-based specifications to ensure system stability without required detailed modeling and analysis is reviewed.

A. Low frequency Resonance

To verify the system modeling and analysis methods presented in this work, a laboratory setup was built and used to test PSUs under different conditions. The setup is depicted in Fig. 10. The Y-connected PSUs are powered from a 30-kVA three-phase programmable power source. Due to its high power rating relative to the PSUs, the output impedance of the programmable source is much lower than the PSU input impedance and will be ignored in system stability analysis.

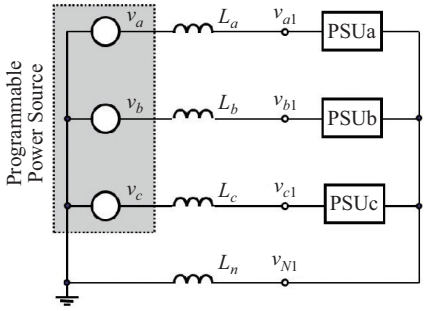

Fig. 10. Laboratory setup used to measure three Y-connected PSUs.

The inductors $L_{\rm a}$, $L_{\rm b}$, $L_{\rm c}$ and $L_{\rm n}$ shown in Fig. 10 are additional inductors purposely inserted to vary the equivalent source impedance seen by the PSUs. A number of experiments were conducted using this setup. In one set of experiments, a 43-mH inductor ($L_{\rm n}$) was inserted in the neutral while no phase inductors were added. The three-phase voltages and currents started to oscillate when the PSU output power is increased to certain level. Fig. 11(a) shows the measured input voltage and current responses when each PSU output power reached 2 kW. A low frequency oscillation similar to that measured in Meta data centers (see Fig. 1 in Part I) can be observed. Fig. 11(b) shows the spectrum of phase a current corresponding to the measured waveforms. The Fourier analysis is performed over a 1-second window to give a frequency resolution of 1 Hz. The magnitude of each harmonic is given in percentage of the fundamental and the fundamental current is excluded in the plot to avoid confusion. Spectra of other phases are similar.

The most significant harmonics in Fig. 11 are at 54 Hz and 66 Hz. To compare with impedance-based stability analysis, note first that the 43-mH inductor in the neutral corresponds to 130 mH in the zero sequence and 43 mH in both positive and negative sequence. Since the PSU admittance is independent of the sequence, the zero sequence is expected to become unstable first under this test condition. Fig. 17 in Part I compared the PSU input impedance against this source impedance. The figure is repeated here in Fig. 12 for easy reference. An unstable resonance at 66 Hz can be concluded from the impedance responses, which corresponds to the measured harmonic at 66 Hz. The 54 Hz harmonic is the

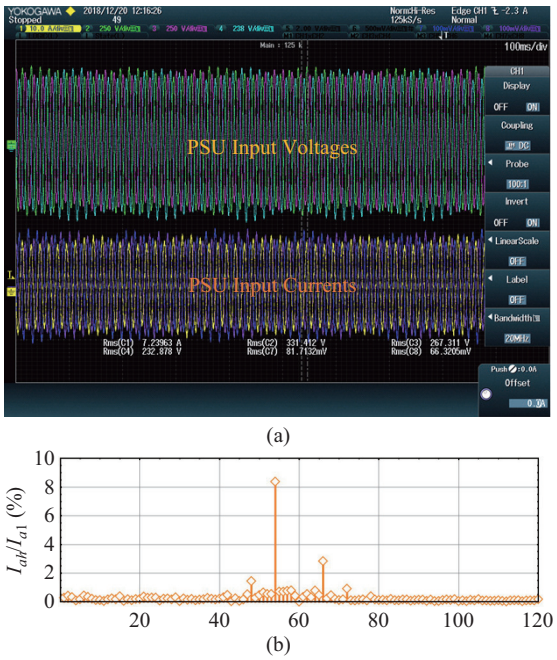

Fig. 11. (a) PSU input voltages and currents when a low frequency resonance starts; (b) phase a current spectrum.

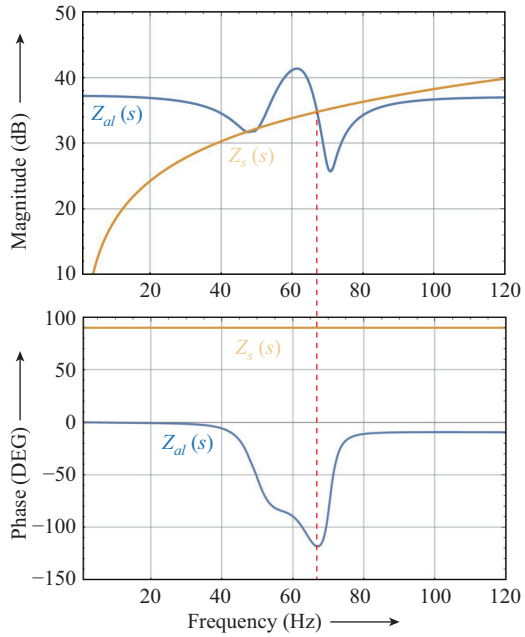

Fig. 12. Impedance analysis of the resonance measured in Fig. 11.

coupled response induced by the 66 Hz resonance through the transfer admittance $Y_{c-2}(s)$ of the PSU.

To verify that the measured resonance at 66 Hz is indeed in the zero sequence, the sequence of the measured three-phase current harmonics are determined at each frequency. The results are summarized in Table II. As can be seen, the harmonic at 66 Hz is mostly in the zero sequence, indicating that the resonance started in the zero sequence. The induced 54 Hz harmonic is mostly in the negative sequence as expected [24]. Note that the fundamental is in the positive sequence.

TABLE II
SEQUENCE OF CURRENT HARMONICS MEASURED IN FIG. 11

Frequency	Zero Seq.	Positive Seq.	Negative Seq.
54 Hz	0.089 A	0.056 A	0.989 A
60 Hz	0.209 A	10.624 A	0.403 A
66 Hz	0.451 A	0.054 A	0.154 A

Actual data center measurements during low frequency resonance events were also collected and processed to verify the proposed system stability analysis method. Fig. 13 shows one set of MSB current measurements and the spectra of the currents. A pair of harmonics at 49 Hz and 71 Hz can be seen in all phase currents. System stability analysis was performed using the PSU impedance models presented in Part I and estimated data center network impedance, as presented in Fig. 14. The equivalent source impedance intersects with the PSU impedance at four different frequencies. Of them, the ones at 49 and 71 Hz are unstable, which corresponds to the measured current harmonic frequencies.

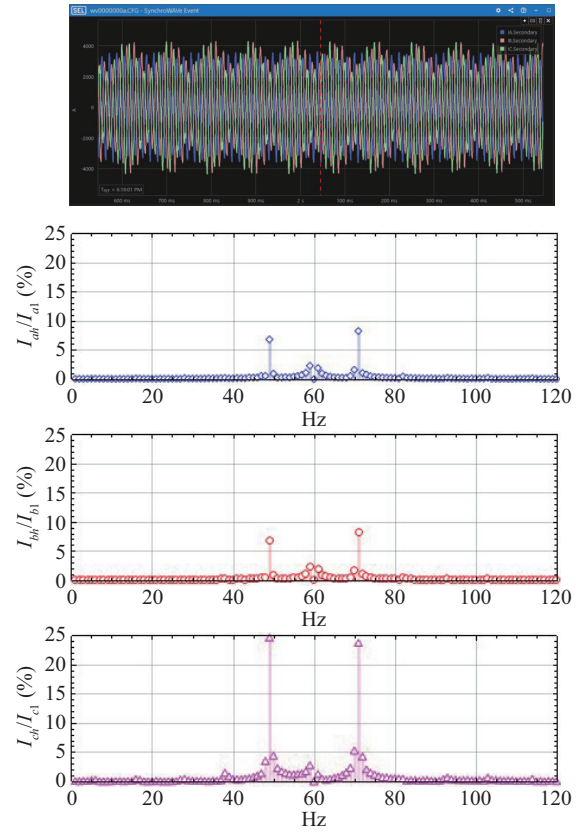

Fig. 13. Waveforms and harmonics of MSB currents measured during a data center resonance.

B. Effects of Phase Unbalance

So far, we have assumed that the network and loads are balanced such that there is no sequence coupling. While transmission line and substation transformer impedances are highly balanced, it is difficult to maintain perfect phase balance in the distribution network due to physical constrains of the building system and other considerations. To keep the analysis simple and practical, it is highly desirable to ignore such unbalance. On the other hand, it is also important to understand

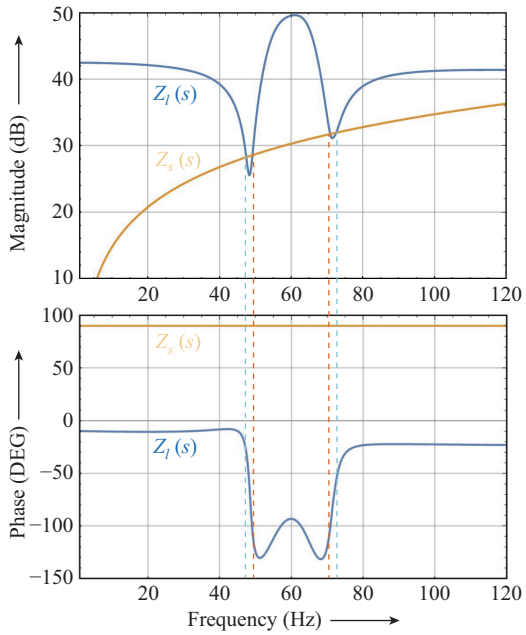

Fig. 14. Impedance analysis of measured data center resonance shown in Fig. 13.

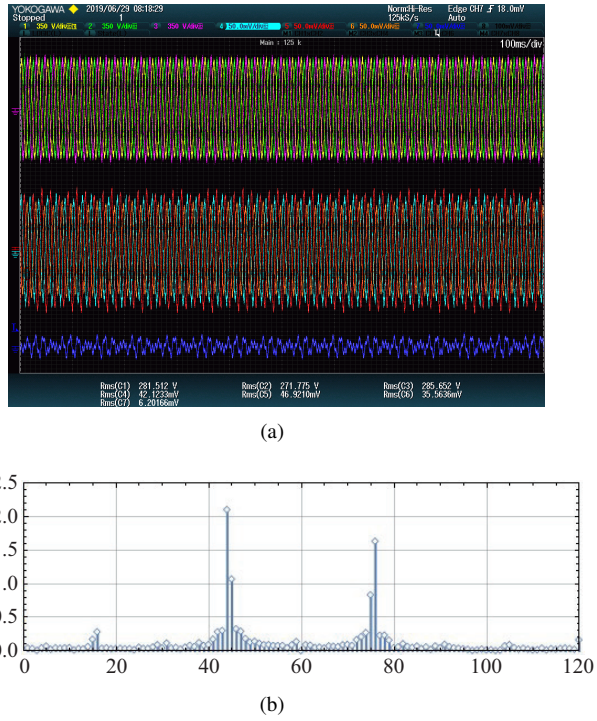

Fig. 15. Operation of Y-connected PSUs with unbalanced source impedance; (a) waveforms; (b) current spectrum.

the effects and to make sure that the simplified models are robust against such un-modeled characteristics.

The mathematic tool we used to quantify the effects of phase unbalance is the matrix perturbation theory [26]. In this approach, the difference between an actual ESI matrix and a "symmetrized" approximation is treated as a perturbation. Several theorems from the matrix perturbation theory can be applied to determine how much the eigenvalues may change because of the perturbation. The general conclusion is that the change will be small and bounded if the perturbation is small.

An experiment was also performed using the laboratory setup depicted in Fig. 10 to quantify the effects of phase unbalance on system stability. The experiment started with a 30 mH inductor inserted in the neutral line. The PSUs can operate stably up to 1 kW input per phase under this condition. The experiment is then repeated with variable inductance inserted in phase b and c. Noticeable harmonics start to appear when L_b and L_c are both increased to 10 mH. The measured voltage and current waveforms are given in Fig. 15(a), and the corresponding phase a current spectrum is presented in Fig. 15(b). By ignoring the internal impedance of the AC source, the equivalent sequence source impedance at the fundamental frequency corresponding to the measurement setup ($L_\mathrm{a} = 0, L_\mathrm{b} = L_\mathrm{c} = 10$ mH, $L_\mathrm{n} = 30$ mH) is found to be:

$$\boldsymbol{Z}_{\mathrm{s012}} = \begin{bmatrix} 0. + 36.44j & 0. - 1.26j & 0. - 1.26j \\ 0. - 1.26j & 0. + 2.51j & 0. - 1.26j \\ 0. - 1.26j & 0. - 1.26j & 0. + 2.51j \end{bmatrix} \tag{66}$$

The three-phase impedance matrix can be "symmetrized" by replacing each of $\{L_\mathrm{a}, L_\mathrm{b}, L_\mathrm{c}\}$ by their average (6.7 mH). The corresponding sequence impedance matrix is

$$\boldsymbol{Z}_{\mathrm{s012}} = \begin{bmatrix} 0. + 36.44j & 0. & 0. \\ 0. & 0. + 2.51j & 0. \\ 0. & 0. & 0. + 2.51j \end{bmatrix} \tag{67}$$

The diagonal elements in (67), which are the same as in (66), correspond to 96.7 mH source inductance in the zero sequence and 6.7 mH in both positive and negative sequence. The off-diagonal elements in (66) correspond to 3.3 mH mutual inductance and represent the difference between the exact and the approximate source impedance models, which is very small despite the large unbalance in the original source impedance matrix. The observed resonance can be predicted by using 96.7 mH as the source impedance, confirming that the approximate balanced ESI matrix is an acceptable simplification for practical system stability analysis.

C. Impedance-Based Specifications for System Stability

The models and methods presented in this work have made it possible to assess practical data center power system stability. They have been successfully used to characterize and solve resonance problems in Meta data centers. A number of new data center designs have also been evaluated using the proposed methods to determine if there might be stability concerns.

As in any large engineered system, solving a stability problem in a data center power system after the fact is highly undesirable because it disrupts operation. Solutions, especially those requiring hardware changes, are also limited and more difficult and expensive to implement in a data center that is already in operation. Stability analysis during the design phase can avoid this problem but may delay the design process and construction if a major change is required to address a stability concern. The most desirable solution, therefore, is to provide

design guidelines and product performance specifications that, when followed and met, can guarantee system stability. To that end, we have developed impedance-based specifications for Meta data centers based on the theory and methods presented in this work. The specifications cover PSU [20], the building power distribution system [21], and UPS [22].

The general approach we follow to develop these specifications relies on sufficient conditions for system stability based on the Nyquist criterion. This is usually how impedance-based specifications are developed [18], [19]. The key is to avoid overly conservative requirements that may compromise other design objectives for data center power systems, such as reliability, efficiency and cost. Practicality and technical feasibility to comply with the requirements are also an important consideration and require a close collaboration with suppliers and other stakeholders. The main requirements we developed are reviewed below.

The specifications we developed for PSU [20] and UPS (input impedance) [22] follow the same approach and are similar in many regards. The requirements comprise three main parts, as outlined below where f_1 denotes the fundamental frequency:

- *Magnitude Response below* $2f_1$: DC bus voltage control causes magnitude dipping as well as negative damping in PSU and UPSinput impedance. Since the negative damping cannot be eliminated, the specs focus on the magnitude response below the second harmonic frequency and require the impedance magnitude not to drop below a certain level relative to the fundamental base impedance of the converter. The expanded two-line system model presented in Section V made it possible to include UPS in system stability analysis such that the developed requirements can cover both PSU and UPS.
- *Operation with Source Impedance*: The limitation on magnitude dipping does not account for the coupled current and the additional dipping it may cause. As an additional measure to assure low frequency stability, PSU and UPS are required to operate resonance-free when additional inductance is inserted at their input to emulate the equivalent source impedance expected in Meta data centers. The added inductance is specified by a BIR (σ) defined in (49), and the BIR value is determined based on Meta data center design.
- *Positive Damping above* $2f_1$: Above the second harmonic frequency, PSU and UPS input impedance exhibit multiple peaks and dips because of resonances of the input filter, as well as negative damping due to control delay. This makes it difficult to control the magnitude. Since high frequency resonance is usually DM resonance and the corresponding ELI varies over a wide range, solutions based on magnitude limitation will not be effective and reliable. Based on these considerations, the specs focus on the phase response and require the impedance to be positively damped above $2f_1$.

Impedance of the distribution network is passive, but high impedance magnitude may cause low frequency resonance. Consistent with the requirements for PSU and UPS, a minimal BIR ($\sigma_{\min}$) is defined for the overall data center distribution system and used as the basis to develop impedance requirements for different components. The value of $\sigma_{\min}$ is set slightly higher than the BIR used to calculate the inserted inductance for PSU and UPS testing to account for phase unbalance and other secondary effects [21].

The minimal BIR is also used to define the upper limit for UPS output impedance below $2f_1$ [22]. Above the second harmonic frequency, the UPS output impedance is subject to the same positive damping requirement as PSU input impedance is.

The requirements we developed also include margins to account for secondary effects that are difficult to measure and control, such as phase unbalance discussed in the previous subsection. Additionally, the specifications include test setup, procedures as well as recommended instrumentation and data processing methods.

To ensure that the requirements can be met in practice, the team has worked with Meta suppliers over the last three years to qualify their products for compliance and demonstrate that the requirements are practically feasible. The specs are in effect now and required for Meta new data centers.

VII. Summary

Part II of this work complemented Part I and presented a set of practical methods to study data center power system stability. The first system model is developed by modeling the distribution network as an equivalent source impedance. Transformation of the three-phase system model into the sequence domain avoids the need for the generalized Nyquist criterion and makes it easy to determine system stability. An expanded system model is also presented to allow network asymmetry, uneven loading and other non-ideal effects to be included in system stability analysis. The general yet simple form of these system models, together with the PSU impedance models developed in Part I, has made it possible to study the stability of practical data center power systems, identify root causes to common problems, and develop effective solutions at both the component and system level.

The analyses presented in Part II also led to a number of general conclusions and recommendations:

- For data centers using Y-connected PSUs, zero sequence is the weakest and the first to become unstable. Design of the distribution network should be optimized to reduce zero-sequence impedance, thereby improving system stability.
- Network asymmetry and uneven loading among parallel lines reduces system stability at low frequency. To improve system stability, the distribution network should be laid out as symmetrically and loaded as evenly as practical.
- In addition to CM resonance with the equivalent source impedance that involves the whole distribution network, PSUs and UPSs in different parts of a data center may also form DM resonance with the network between them.
- A low-frequency resonance (below the second harmonic frequency) is most likely a CM resonance caused by a

high ESI, while a high frequency resonance that does not involve a UPS is usually a DM resonance.

- Negative damping in PSU and UPS impedance is the common root cause for system resonance but requires different solutions in different frequency ranges.
- A low-frequency resonance can be solved by avoiding dipping in the PSU and UPS input impedance magnitude. This can usually be achieved by having sufficient phase margin in DC voltage control (and PLL in UPS, if used.)
- The magnitude of PSU and UPS impedance as well as the ELI varies significantly at high frequency and is difficult to control. Avoiding high-frequency resonance should focus on the phase response.

Based on the models and analyses presented in this work, new design guidelines and product performance specifications have been developed for Meta data centers to ensure system stability by design. The specs serve also as a useful reference for the data center industry as well as other industries.

REFERENCES

[1] J. Sun, M. Xu, M. Cespedes, D. Wong, and M. Kauffman, "Data center power system stability – Part I: power supply impedance modeling," *CSEE Journal of Power and Energy Systems*, doi: 10.17775/CSEEJPES.2021.02010.

[2] Data Center Map, Baxtel. [Online]. Available: https://baxtel.com/map

[3] A. Pratt, P. Kumar, and T. V. Aldridge, "Evaluation of 400V DC distribution in Telco and data centers to improve energy efficiency," in *Proceedings of the 29th International Telecommunications Energy Conference*, 2007, pp. 32–39.

[4] L. Schrittwieser, J. W. Kolar, and T. B. Soeiro, "99% efficient three-phase buck-type SiC MOSFET PFC rectifier minimizing life cycle cost in DC data centers," *CPSS Transactions on Power Electronics and Applications*, vol. 2, no. 1, pp. 47–58, Jul. 2017.

[5] J. Park, Data Center – Mechanical Specifications v1.0. [Online]. Available: https://www.opencompute.org/wiki/Data_Center/SpecsAndDesigns

[6] A. Kusko, D. Galler, and N. Medora, "Output impedance of PWM UPS inverter-feedback vs. filters," in *Conference Record of the 1990 IEEE Industry Applications Society Annual Meeting*, Seattle, WA, USA, 1990, pp. 1044–1048.

[7] D. Stanojevic and M. Stefanovic, "A UPS inverter with zero output impedance," in *Proceedings of IECON'94 - 20th Annual Conference of IEEE Industrial Electronics*, Bologna, Italy, 1994, pp. 469–472.

[8] J. Sun, M. J. Li, Z. G. Zhang, T. Xu, J. B. He, H. J. Wang, and G. H. Li, "Renewable energy transmission by HVDc across the continent: system challenges and opportunities," *CSEE Journal of Power and Energy Systems*, vol. 3, no. 4, pp. 353–364, Dec. 2017.

[9] J. Adams, C. Carter, and S. H. Huang, "ERCOT experience with sub-synchronous control interaction and proposed remediation," in *PES T&D 2012*, 2012, pp. 1–5.

[10] I. Vieto, G. H. Li, and J. Sun, "Behavior, modeling and damping of a new type of resonance involving type-III wind turbines," in *Proceedings of the 2018 IEEE 19th Workshop on Control and Modeling for Power Electronics (COMPEL)*, Padova, Italy, 2018, pp. 1–8.

[11] C. Buchhagen, M. Greve, A. Menze, and J. Jung, "Harmonic stability-practical experience of a TSO," in *Proceedings of the 2016 Wind Integration Workshop*, Vienna, 2016, pp. 1–6.

[12] H. Saad, Y. Fillion, S. Deschanvres, Y. Vernay, and S. Dennetière, "On resonances and harmonics in HVDC-MMC station connected to AC grid," *IEEE Transactions on Power Delivery*, vol. 32, no. 3, pp. 1565–1573, Jun. 2017.

[13] J. Sun, I. Vieto, and C. Buchhagen, "High-frequency resonance in HVDC and wind power systems: root causes and solutions," *IET Renewable Power Generation*.

[14] J. Sun, "Impedance-based stability criterion for grid-connected inverters," *IEEE Transactions on Power Electronics*, vol. 26, no. 11, pp. 3075–3078, Nov. 2011.

[15] H. Wang, W. Mingli, and J. J. Sun, "Analysis of low-frequency oscillation in electric railways based on small-signal modeling of vehicle-grid system in *dq* frame," *IEEE Transactions on Power Electronics*, vol. 30, no. 9, pp. 5318–5330, Sep. 2015.

[16] H. Wang, C. Buchhagen, M. Greve, and J. Sun, "Methods to aggregate turbine and network impedance for wind farm resonance analysis," in *Proceedings of the 17th Wind Integration Workshop*, Stockholm, 2018, pp. 1–8.

[17] W. Dong, H. H. Xin, D. Wu, and L. B. Huang, "Small signal stability analysis of multi-infeed power electronic systems based on grid strength assessment," *IEEE Transactions on Power Systems*, vol. 34, no. 2, pp. 1393–1403, Mar. 2019.

[18] C. M. Wildrick, F. C. Lee, B. H. Cho, and B. Choi, "A method of defining the load impedance specification for a stable distributed power system," *IEEE Transactions on Power Electronics*, vol. 10, no. 3, pp. 280–285, May 1995.

[19] R I-20005, Anforderungen an die Eingangs-Admittanz von Umrichter-triebfahrzeugen, SBB, 2013.

[20] M. Cespedes and H. Keyhani, "Data center system stability requirements for power supplies," presented at *2020 OCP Global Summit*, 2020.

[21] M. Mihret, "Data center electrical spec for system stability," presented at *2020 OCP Global Summit*, 2020.

[22] M. Cespedes, "Development of system specifications for UPS," presented at *2020 OCP Global Summit*, 2020.

[23] M. Cespedes and J. Sun, "Impedance modeling and analysis of grid-connected voltage-source converters," *IEEE Transactions on Power Electronics*, vol. 29, no. 3, pp. 1254–1261, Mar. 2014.

[24] J. Sun, "Sequence impedance modeling and analysis of wind and PV inverters considering coupling over frequency," presented at *IEEE ECCE 2018*, Portland, OR, 2018.

[25] H. J. Wang and J. Sun, "Impedance-based stability modeling and analysis of networked converter systems," in *Proceedings of the* 2019 *20th Workshop on Control and Modeling for Power Electronics (COMPEL)*, Toronto, Canada, 2019, pp. 1–8.

[26] G. W. Stewart and J. G. Sun, *Matrix Perturbation Theory*, Boston: ACademic Press, 1990.

Jian Sun received the B.S. degree from Nanjing Institute of Aeronautics, Nanjing, China, the M.S. degree from Beijing University of Aeronautics and Astronautics, Beijing, China, and the Dr. Eng. degree from University of Paderborn, Germany, all in electrical engineering.

Dr. Sun was a Post-Doctoral Fellow with the School of Electrical and Computer Engineering, Georgia Institute of Technology, from 1996 to 1997. From 1997 to 2002, he worked in the Advanced Technology Center of Rockwell Collins, Inc., where he led research on advanced power conversion for aerospace applications. In August 2002, he joined Rensselaer Polytechnic Institute in Troy, NY where he is currently a Professor and Director of the New York State Center for Future Energy Systems (CFES). His research interests are in the general area of power electronics and energy conversion, with a focus on modeling, control, as well as applications in aerospace and renewable energy systems. He has published more than 200 journal and conference papers on these subjects, and holds 12 US and European patents.

Dr. Sun is a Fellow of IEEE. He received the PELS Modeling and Control Technical achievements Award in 2013 and the R. David Middlebrook Outstanding achievement Award in 2017. He served as the Editor-in-Chief of the IEEE Power Electronics Letters from 2008 through January 2014, and is currently the Vice President of Conferences of the IEEE Power Electronics Society (PELS). He has also served PELS in a number of other positions, including Chair of the Technical Committee on Power and Control Core Technologies, Member at Large of the AdCom, Technical Program Co-Chairs of ECCE, Distinguished Lecture, and Treasurer.

Melaku M. Mihret received the B.S. degree from Addis Ababa University, Ethiopia and the M.S. degree from Tennessee Technological University, USA, both in electrical engineering. From 2011 to 2012, he worked at Cummins Inc. as Electronic Systems Engineer. Between 2012 and 2018, he worked as Lead Power Electronics Engineer at Aggreko/Younicos designing power converters for battery energy storage applications and microgrid controls. Since 2018, he has been with Meta Platforms Inc. as Data Center Systems Engineer working on electrical system designs for data centers.

Mauricio Cespedes received the B.S. degree from the University of Costa Rica, and the M.S. and Ph.D. degrees from Rensselaer Polytechnic Institute in Troy, NY, USA, all in electrical engineering. From 2014 to 2018, he was with Enphase Energy Inc. as a senior staff power electronics control engineer. Since 2018, he has been with Meta Platforms Inc. as a data center systems engineer working on data center power quality and stability. Dr. Cespedes was a recipient of two best paper awards from the IEEE Transactions on Power Electronics, and he is a member of IEEE PELS.

David Wong joined Meta Platforms Inc. data center organization in 2017, supporting the Systems Engineering and Operations Integration teams for stable, scalable, and efficient deployment and data center operations. Prior to working at Meta, he held technical management roles at Infinera developing optical transport products for telecom carriers and data centers. He also held an engineering management role at Force10 Networks (acquired by Dell) developing leading edge networking products. He received B.S. degree from the San Jose State University in Computer Engineering and completed the Advanced Leadership Program at Stanford University in Graduate School of Business.

Mike Kauffman received the B.S. degree from the University of Cincinnati, and the M.S. and Ph.D. degrees from Stanford University, all in electrical engineering. Since 2016, he has been with Meta Platforms Inc., supporting engineering teams in the data center organization. Prior to working at Meta, he developed fiber optic telecommunications equipment at Infinera, storage networking equipment at Gadzoox Networks, and high frequency radios at Hewlett-Packard Labs.